W

SACLANT ASW
RESEARCH CENTRE

THE INFLUENCE OF A LOW VELOCITY LAYER ON THE REFLECTIVITY
FROM THE SEA FLOOR

by

OLE. F. HASTRUP

15 MAY 1966

NATO ─────────────────────

TECHNICAL REPORT NO. 61

SACLANT ASW RESEARCH CENTRE
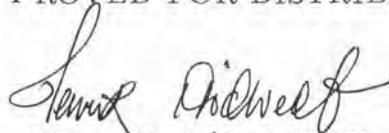
Viale San Bartolomeo 92

La Spezia, Italy

THE INFLUENCE OF A LOW VELOCITY LAYER ON THE REFLECTIVITY

FROM THE SEA FLOOR

By

Ole F. Hastrup

15 May 1966

APPROVED FOR DISTRIBUTION

HENRIK NØDTVEDT

Director

Manuscript Completed:

16 March 1966

TABLE OF CONTENTS

THE INFLUENCE OF A LOW VELOCITY LAYER ON THE REFLECTIVITY FROM THE SEA FLOOR

By

Ole F. Hastrup

ABSTRACT

The influence on the reflectivity of a low velocity layer on top of a sand half-space has been investigated. By expressing sediment density and velocity in terms of porosity it has been possible to use this quantity as an independent variable. To characterize the reflectivity, both the reflection loss in decibels and the distortion after reflection of two broad band pulses have been used. The calculations were carried out on a digital computer and the results are presented in the form of curves and graphs.
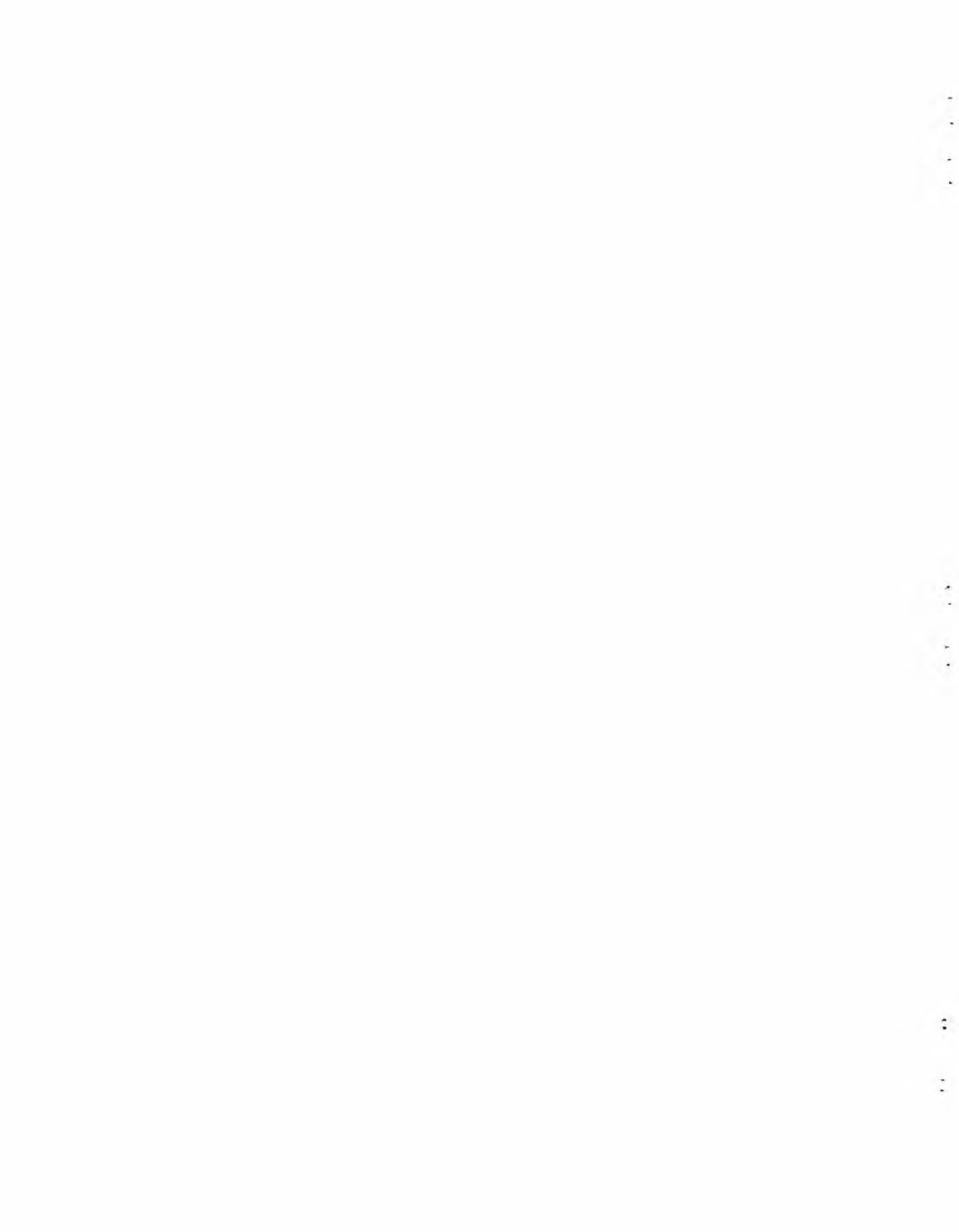
INTRODUCTION

On the sea floor a poorly consolidated sedimentary layer is very often found on top of a more solid bottom. Because of the usually high porosity of such a layer, the sound velocity might be lower there than in the surrounding layers. Therefore, the layer has no critical angle, but instead has an intromission angle at which very large reflection losses can occur. There is thus a certain interest for bottom-bounce sonar studies in making a detailed investigation of the influence of the elastic parameters of such a low velocity layer on its reflectivity.

By using porosity as a variable, and relating density and sound velocity to this quantity, it is possible to reduce the number of independent parameters. To characterize the reflectivity, use is made of both the reflection coefficient and the reflection of broad band sources. A brief description of the analytical and numerical methods used for their calculation are given in the Appendix.

1. THE RELATIONSHIP BETWEEN VELOCITY-DENSITY AND POROSITY

For a poorly consolidated sediment with a high porosity it is valid to assume a fluid-like behaviour; it is therefore possible to set up equations relating sound-velocity and density with porosity.

The porosity of a sediment is defined as the ratio between the volume of the voids and the total volume of the sediment. We assume (Refs. 1 & 2) that we can treat the sediment as an ideal two-component mixture and that the equations for elastic wave propagation are valid.

If the density of the solid particulate matter in the sediment is constant, then, from the definition of porosity, the bulk sediment density is given by

$$\rho_{sediment} = \rho_{solid}(1-p) + \rho_{water} \cdot p,$$

where ρ is the density and p the porosity. Measurements (Ref. 3) indicate that this relationship is valid in most cases.

The sound velocity for a liquid is given by

$$\alpha = \sqrt{\frac{1}{\rho B}}$$

where B is the compressibility. We assume that B can be expressed as the sum of the two component moduli, so, in terms of the porosity, we get

$$B_{sediment} = B_{solid} \cdot (1-p) + B_{water} \cdot p$$

3

By inserting into the velocity equation, and using the value for ρ_{sed}, we can get the ratio between the sediment and water sound velocity as

$$\alpha_{sed.} \Big/ \alpha_{water} = \sqrt{\dfrac{1}{\left[\dfrac{\rho_{solid}}{\rho_{water}}(1-p)+p\right]\left[\dfrac{B_{solid}}{B_{water}}(1-p)+p\right]}}$$

Using $\rho_{solid} \Big/ \rho_{water} = 2.62$, and $B_{solid} \Big/ B_{water} = 0.0466$, the values of $\rho_{sediment} \Big/ \rho_{water}$ and $\alpha_{sediment} \Big/ \alpha_{water}$ have been calculated; the results are shown in Fig. 1. Measurements of the sound velocity in the sediments and of the porosity indicate that the assumptions made seem to be valid. (Ref. 4). An interesting thing about the sediment velocity is that there is a minimum of 78% porosity with a relative sound velocity of only 0.966.

In the case of reflection from a layer with a lower velocity, no critical angle will be found, because the angle of incidence in water will always be greater than that in the sediment. Rayleigh's formula for the reflection coefficient shows that this becomes zero for

$$\rho_{sediment} \Big/ \rho_{water} = \sqrt{\dfrac{(\alpha_{water} \Big/ \alpha_{sediment})^2 - \sin^2\theta}{1 - \sin^2\theta}}$$

where θ is the angle of incidence. But, as $\rho_{sediment} \Big/ \rho_{water}$ and $\alpha_{water} \Big/ \alpha_{sediment}$ can be expressed by the porosity, we get $\theta = \theta(p)$.

Figure 2 shows θ as a function of porosity in the interval $100\% \geqq p \geqq 57\%$. In the literature this angle is usually called either the Brewster angle or the intromission angle.

4

2.   NUMERICAL CALCULATIONS

2.1   From the cores taken by the Centre it seems that the porosity of the upper layers of the deep sea bed is usually about 75%. It might therefore be of interest to see how a low velocity layer on the top of more consolidated sediments will affect the reflectivity.

It was decided to consider a top layer with porosities ranging from 55% to 100% in steps of 5% (100% porosity is physically unreasonable, but is included for completeness). For the lower layer, medium sand with a porosity of 35% was chosen, and the same constants (Table 1) were used as were used for the second layer in Refs. 5 & 6, where, by choice, α = ρ = 1.00 for the water.

TABLE 1

α	β	a	b	ρ
1.13	0.40	1.5	2.5	2.05

α and β= the velocity of compressional and shear waves

a   and b= the damping of compressional and shear waves, in decibel per wavelength

ρ = density.

To obtain a general picture of the reflection loss, this has been calculated near the minimum velocity in the top layer, using the following relative constants:

5

TABLE 2

α	β	a	b	ρ
0.966	0.05	1.0	1.5	1.36

Figure 3 shows isolines of the reflection loss expressed as a function of the angle of incidence and a wave number — in this case defined as $8d/\lambda$, and therefore dimensionless. The usual system of ridges and valleys corresponds to the multiples of quarter and half wave length ($\lambda/4$ and $\lambda/2$) thicknesses of the top layer, whereas the characteristics of the critical angle in the lower layer are missing except for $8d/\lambda$ less than the order of 1.

To obtain a more visual feeling of how the reflectivity depends on the angle of incidence and the wave number, the reflection loss is shown in Fig. 4 as a three-dimensional display. This has been prepared by plotting the cuts in the surface made by planes corresponding to a series of fixed wave numbers.

2.2 An important question in this case is how does loss depend on porosity and layer thickness, and how does it influence the distortion of reflected shock and bubble pulses?

Table 3 gives the elastic constants used for the low-velocity layer in the cases investigated:

TABLE 3

Porosity %	α	β	a	b	ρ
100	1.000	0.05	1.0	0.05	1.00
95	0.986	0.05	1.0	0.05	1.08
90	0.975	0.05	1.0	0.05	1.16
85	0.969	0.05	1.0	0.05	1.24
80	0.966	0.05	1.0	0.05	1.32
75	0.967	0.05	1.0	0.05	1.41
70	0.971	0.05	1.0	0.05	1.49
65	0.979	0.05	1.0	0.05	1.57
60	0.990	0.05	1.0	0.05	1.65
55	1.006	0.05	1.0	0.05	1.73

The numerical results for vertical incidence are shown in Figs. 5 to 10, together with the limiting loss for $n \to \infty$. In the calculations of frequency, the velocity α = 1.00 has been used in all cases; so with $n = \alpha / \lambda$ and d/λ = q, one gets $n = q \cdot \alpha /d$, where q is a dimensionless number. One must notice that for porosities greater than 60% the absolute maximum reflection loss occurs not at the first quarter wave thickness but at the higher multiples, increasing as the porosity increases. The minimum loss peaks follow the same asymptotic trend as is usually noticed in the case without an intromission angle.

The influence of the low-velocity layer thickness is also of great importance, and the loss curves for angles of incidence of 0°, 40°, 60°, and 80° are plotted on Figs. 11 to 14. In the wavelength/layer-thickness calculations the value of α = 1.00 is again used. To obtain a more simplified picture, the maximum loss

for $0 < (\alpha/d) < 0.5$ is given in Fig. 15 as a function of porosity, a curve being drawn for each of the angles used. Except for the angle of incidence of 80°, there is a very clear maximum loss at around 60% to 70% porosity, the losses here being from 10 dB to 20 dB larger those for 55% porosity.

This shows that when a high frequency harmonic source is used, even a thin low-velocity layer might absorb almost all the signal, even when there is a good reflector underneath.

2.3 The effect on the reflection of a wide-band signal is difficult to predict just by looking at the reflection-loss curves. Therefore the distortion of both a shock and a bubble pulse from an explosion has been used; these pulses are the same as were used in Ref. 6, and are both peaked around a frequency corresponding to $\lambda \sim 4d$. To see the influence of the angle of incidence, the reflection from the model using the data in Tables 1 & 2 has been calculated for angles of incidence of 0°, 20°, 40°, 60°, and 80°; the results are shown in Figs. 16 & 17. The shape does not differ very much for the first four angles, except for the closing-in of the second pulse, whereas after the critical angle in the lowest layer there is a very marked change for both the shock and bubble pulses.

The reason for the catching-up of the second pulse can be explained by the geometrical phase shift in the top layer; this is equal to $k_1 \cos \theta_1 d$, where $k_1 = 2\pi/\lambda$ is the usual wave number, θ_1 is the angle of incidence in the layer, and d_1 is the thickness. The frequency-dependent phase-shift for small angles of incidence is small and oscillates with frequency; therefore, to a great extent, it will cancel out for a wide band source. Table 4 gives the calculated and observed time differences for the shock pulse.

TABLE 4

θ_0	θ_1	$\frac{d}{\alpha_,}\cos\theta_1$	t_{obs}
$0°$	$0°$	1.037	1.04
$20°$	$19°16'$	0.978	0.99
$40°$	$38°23'$	0.812	0.82
$60°$	$56°50'$	0.567	0.57
$80°$	$72°11'$	0.317	0.28

So for $\theta_0 \leq 60°$, the influence of the frequency-dependent phase-shift is of the order of 1%, and increases to 10% for $\theta_0 = 80°$.

Because of the relatively small change in shape from $0°$ to $60°$, the pulse shapes for different porosities have only been calculated for angles of incidence of $0°$ and $80°$. The results are shown in a 3-dimensional plot in Figs. 18-21 to enable a comparison to be made between the shapes for different porosities. The general form does not change for the vertical incidence cases, whereas at $80°$ there is a rather marked difference, e.g. between 80% and 55% porosity.

The influence of the porosity on the amplitudes can be seen in Figs. 22-25, where the different peak amplitudes are plotted as a function of the porosity. In the case of vertical incidence, both peak amplitudes follow an almost linear dependence of porosity. At $80°$ incidence the largest negative pulse shows a minimum in the range of 80%-90% porosity.

CONCLUSION

Summarizing the results given in the previous chapter, the following can be said:

a.   When a low velocity layer is on top of a high velocity layer, the general reflection loss surface at the velocity minimum shows the same characteristics as in the case where an intromission angle does not exist, except for the lack of critical angle for higher frequencies ($\lambda <$ 8d) and a generally higher loss.

b.   The influence of the layer thickness for the chosen model and for angles of incidence at 0°, 20°, 40°, 60° & 80° gives, for d $\sim \lambda / 4$ and 60-70% porosity, a maximum with losses 10-20dB larger than the values for 55%.   Therefore, even a thin layer might reduce the reflections considerably in the case of a high frequency harmonic source.

c.   For vertical incidence, the peak amplitudes for both shock and bubble pulses depend linearly on the porosity.   For 80° angle of incidence the porosities from 80-90% give the smallest amplitudes for the largest negative pulse.

As a general conclusion one can say that a low velocity layer decreases the reflectivity by several decibels and that, for certain angles of incidence and frequency, the loss may be even as high as 30 dB with respect to the case where only the lower layer is present.

REFERENCES

1.   R. J. Urick, J. Appl. Phys. 18 , 983, (1947).

2.   R. J. Urick, J. Acoust. Soc. Am. 20, 283, (1948).

3.   E. L. Hamilton, et al., J. Acoust. Soc. Am. 28, 1, (1956).

4.   E. L. Hamilton, J. Acoust. Soc. Am. 28, 16, (1956).

5.   O. F. Hastrup, "Reflection of Plane Waves from a Solid Multilayered Damping Bottom", SACLANTCEN T. R. No. 50, March 1966, NATO UNCLASSIFIED.

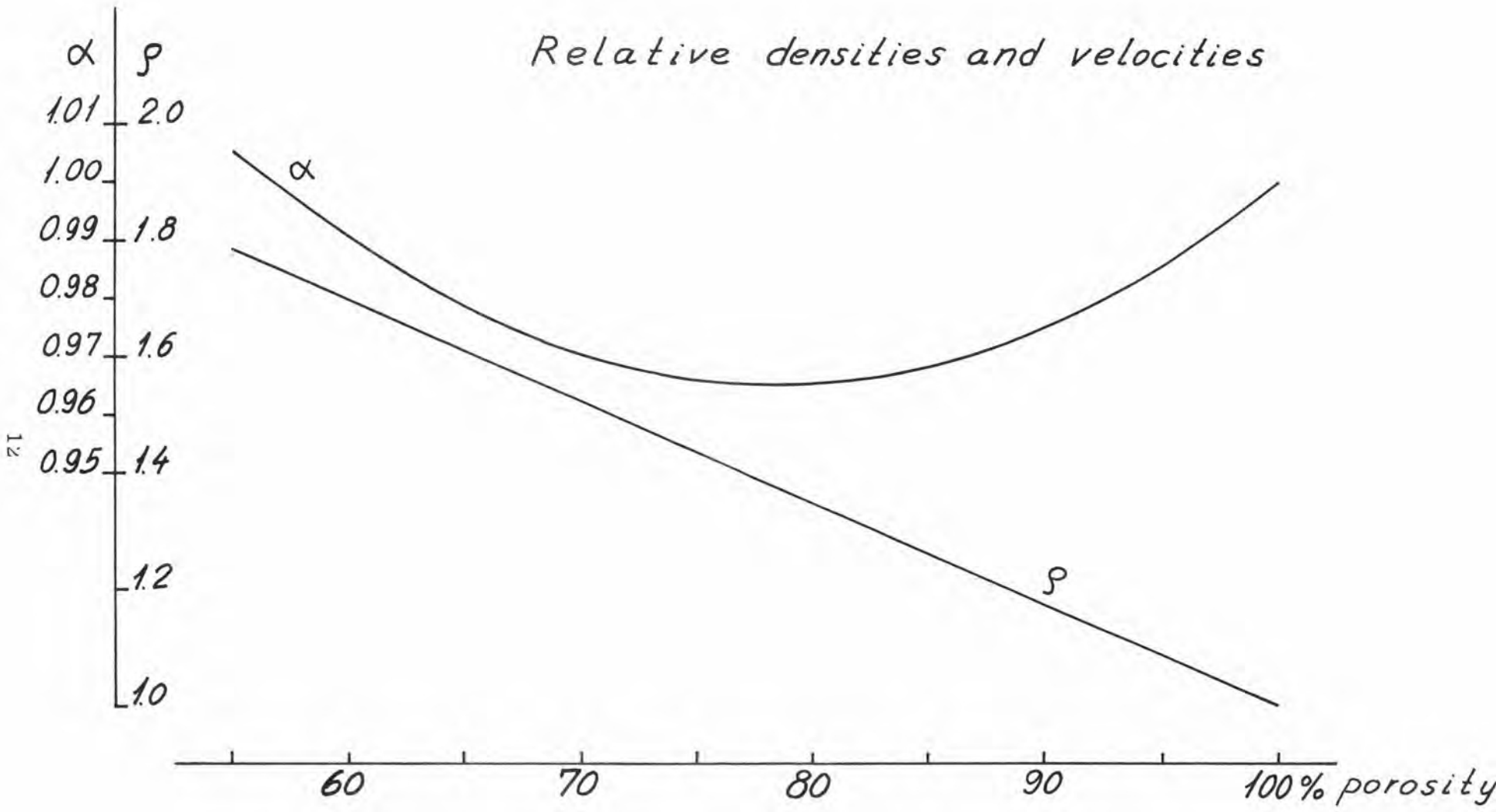6.   O. F. Hastrup, "Distortion of Bottom Reflected Pulses", SACLANTCEN T. R. No. 51, March 1966, NATO UNCLASSIFIED.

FIG. 1 RELATIVE DENSITY AND VELOCITY VERSUS POROSITY
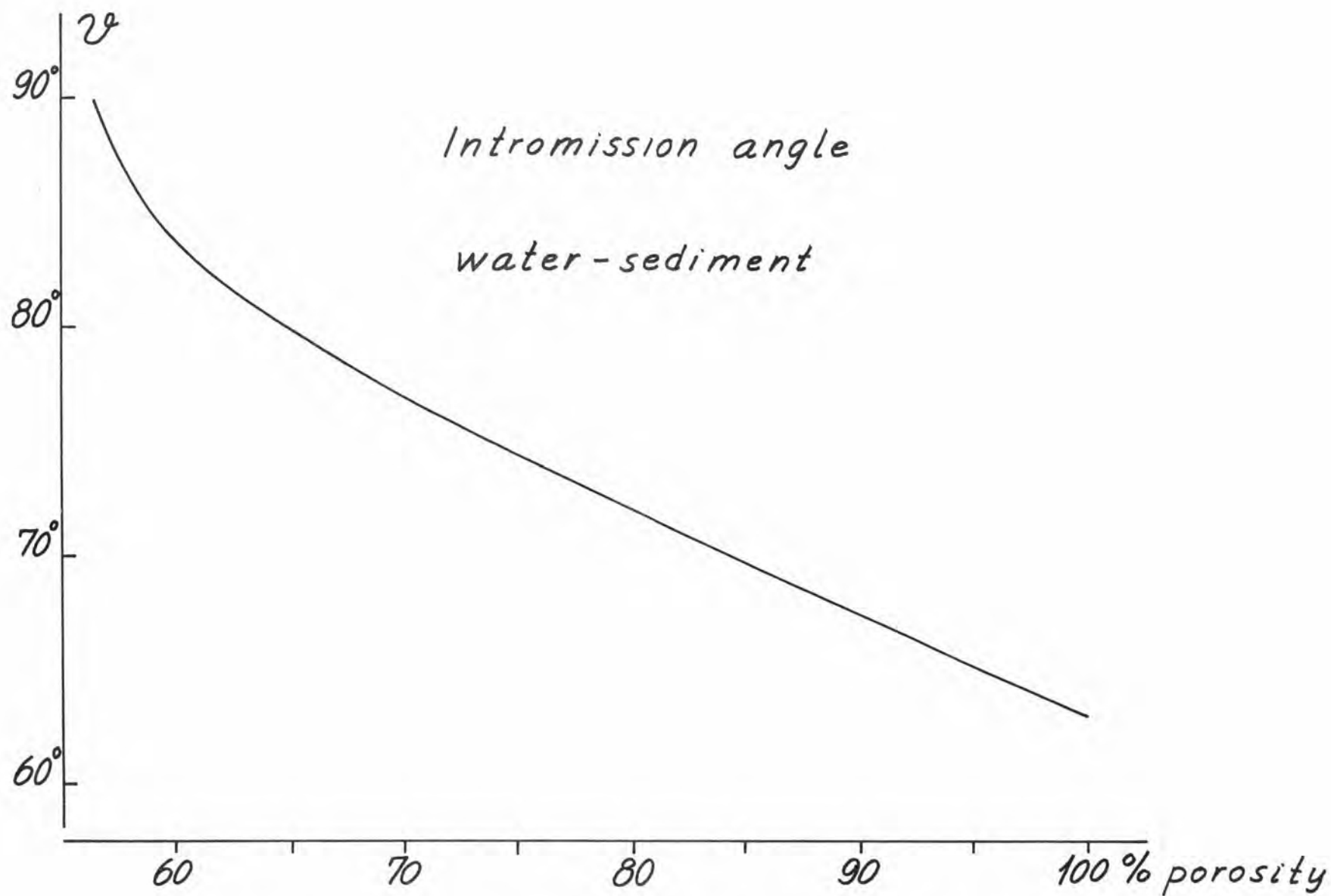
FIG. 2   INTROMISSION ANGLE FOR A BOUNDARY BETWEEN WATER AND A LOW—VELOCITY SEDIMENT
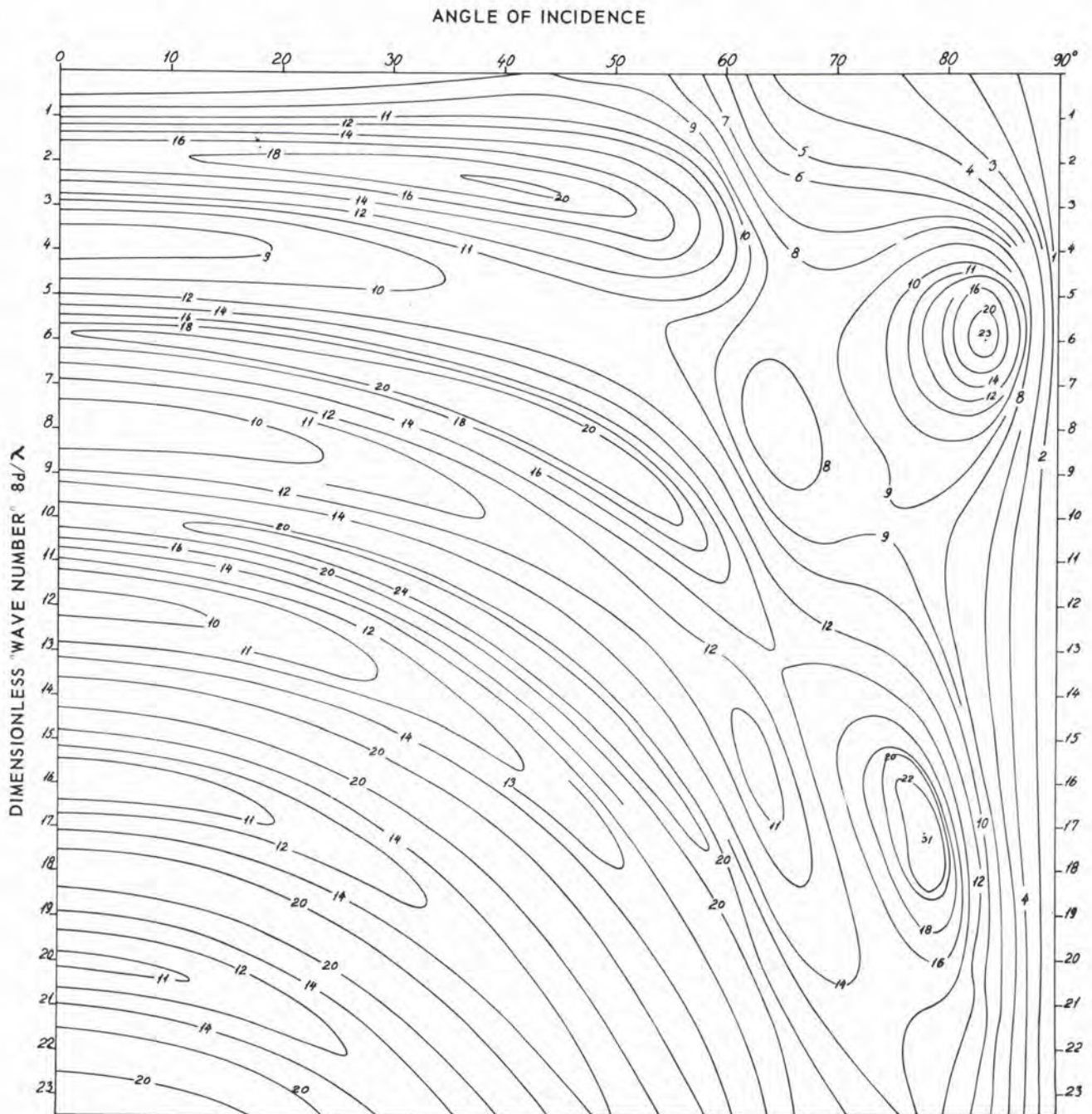
FIG. 3 ISOLOSS LINES AT THE VELOCITY MINIMUM AS A FUNCTION OF FREQUENCY AND ANGLE OF INCIDENCE

14
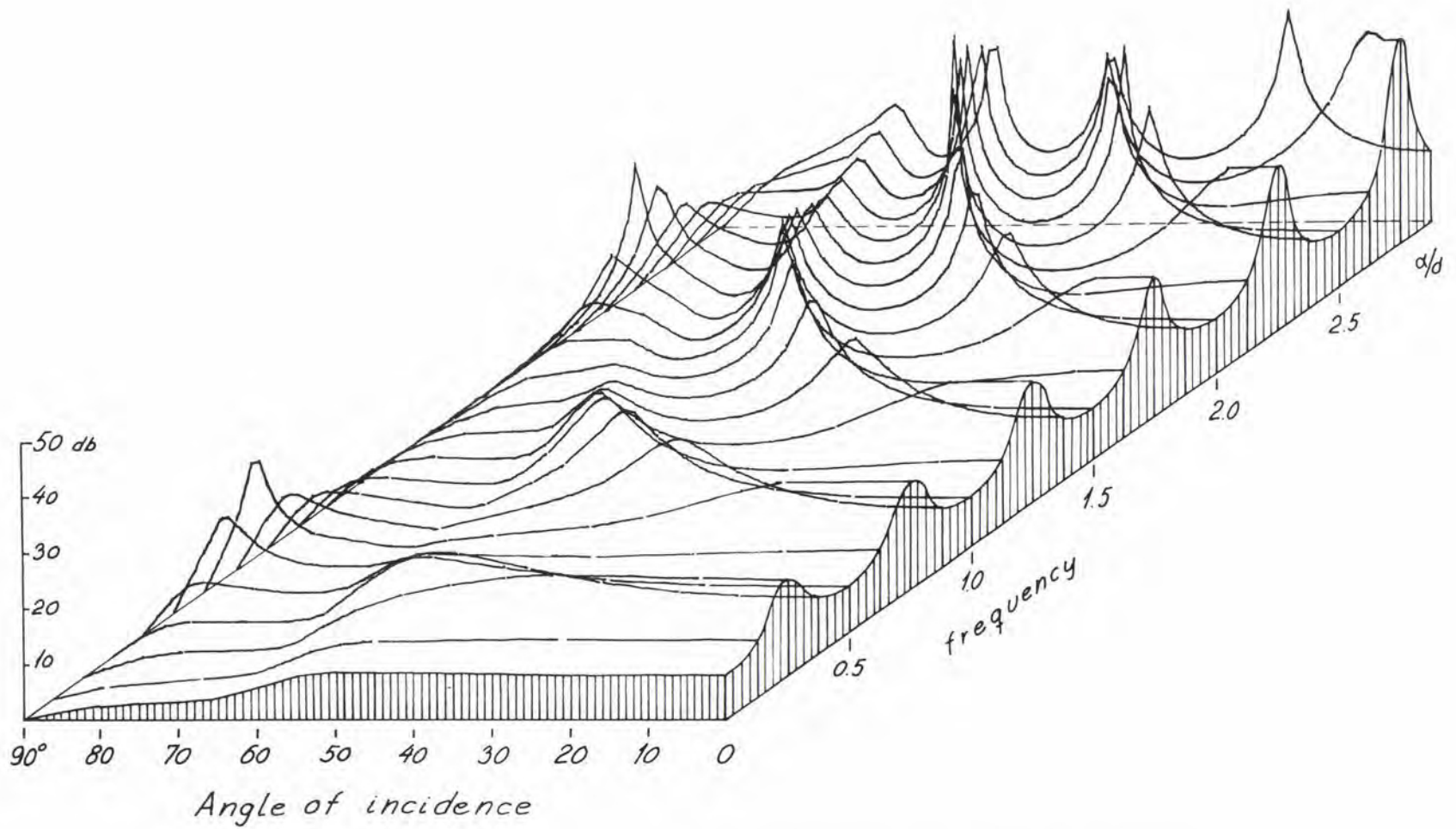
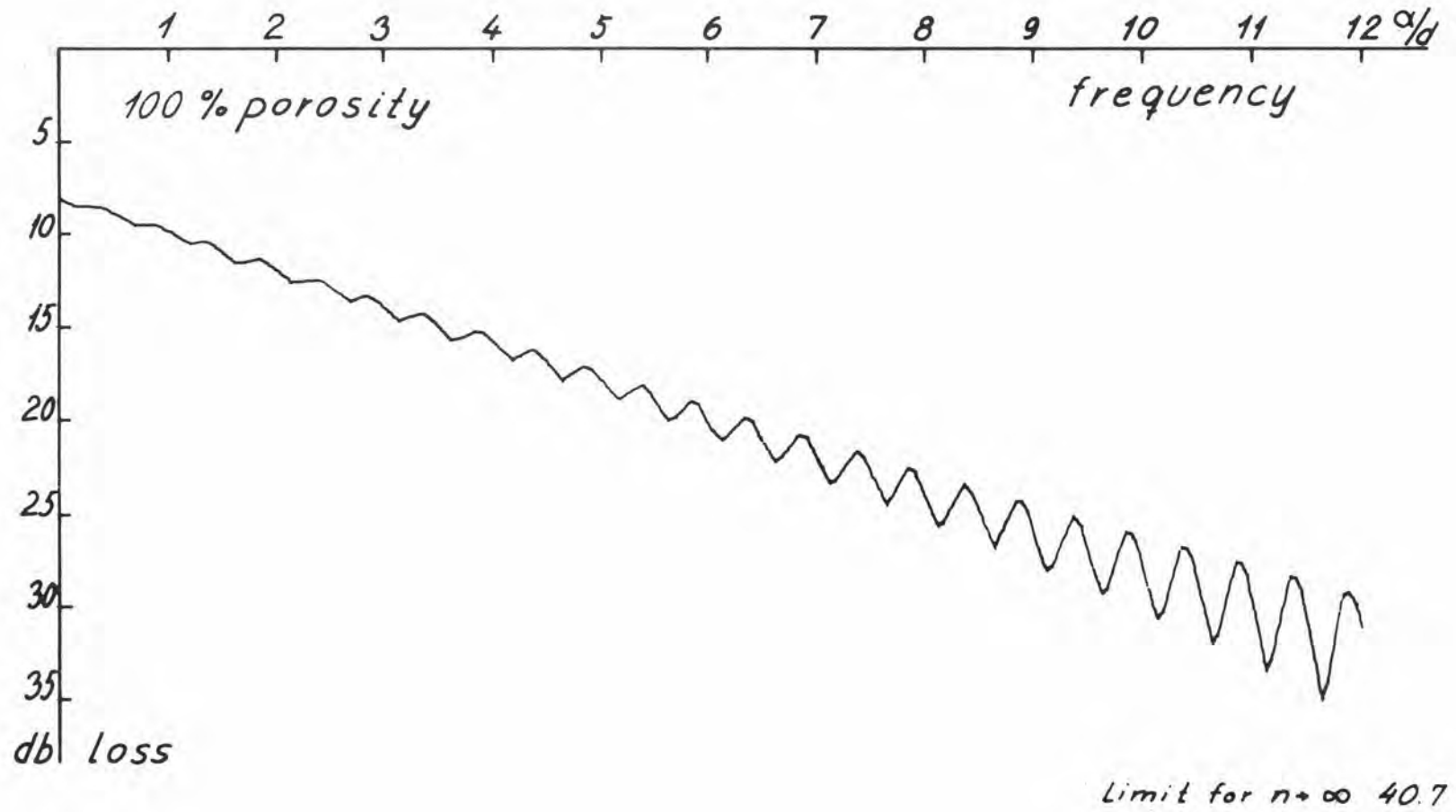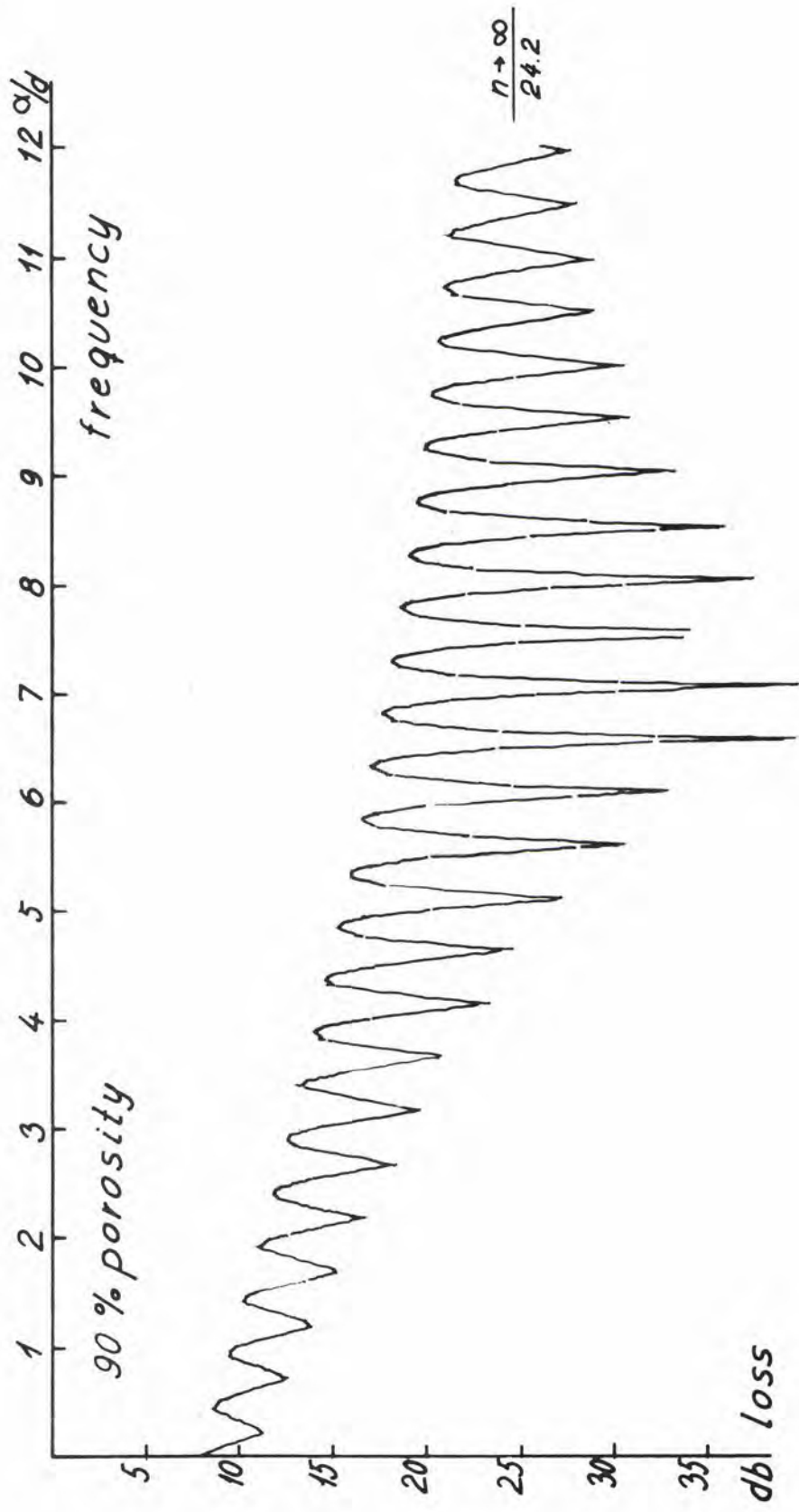FIG. 4 REFLECTION LOSS AS A FUNCTION OF FREQUENCY AND ANGLE OF INCIDENCE

15

FIG. 5 REFLECTION LOSS FOR VERTICAL INCIDENCE

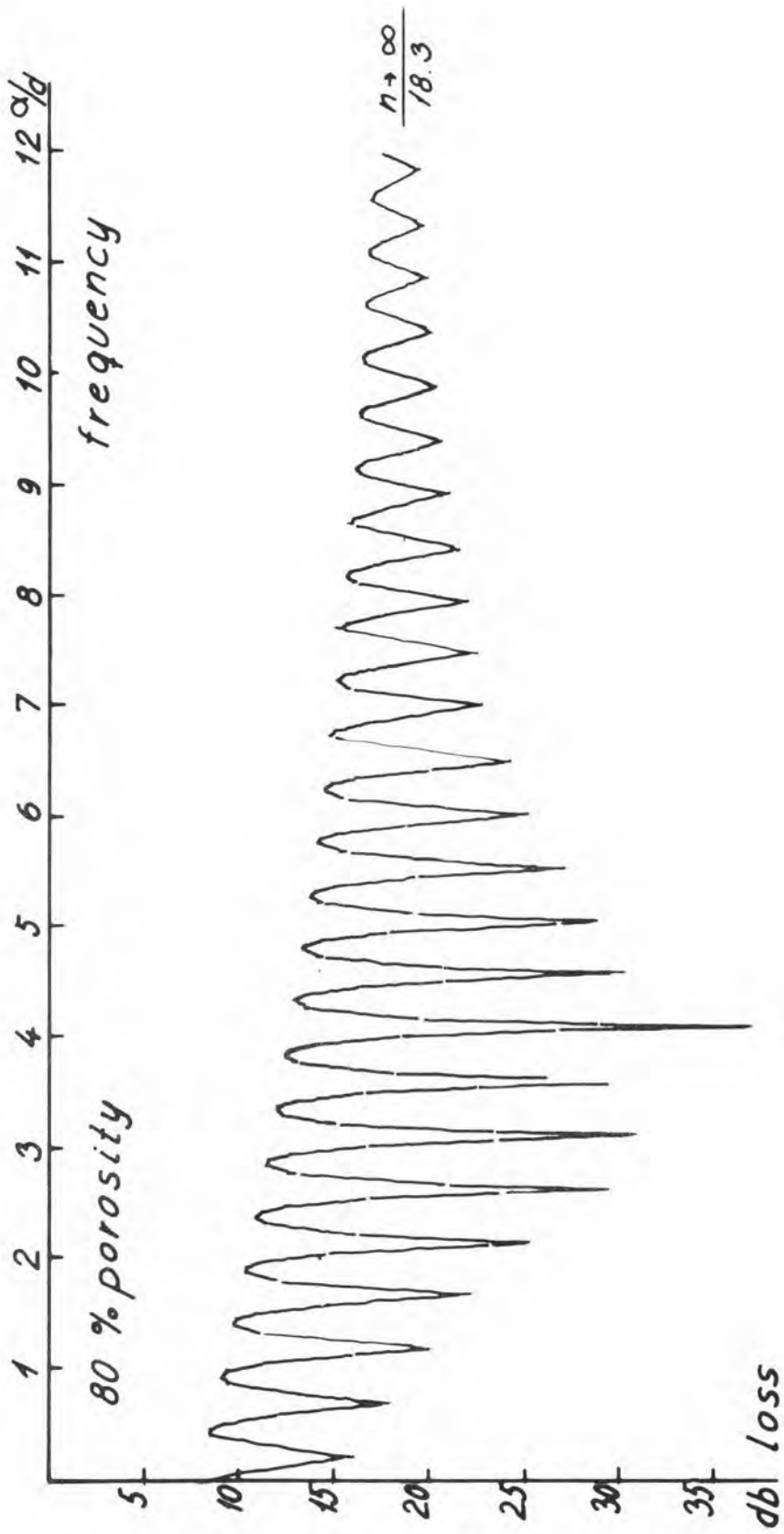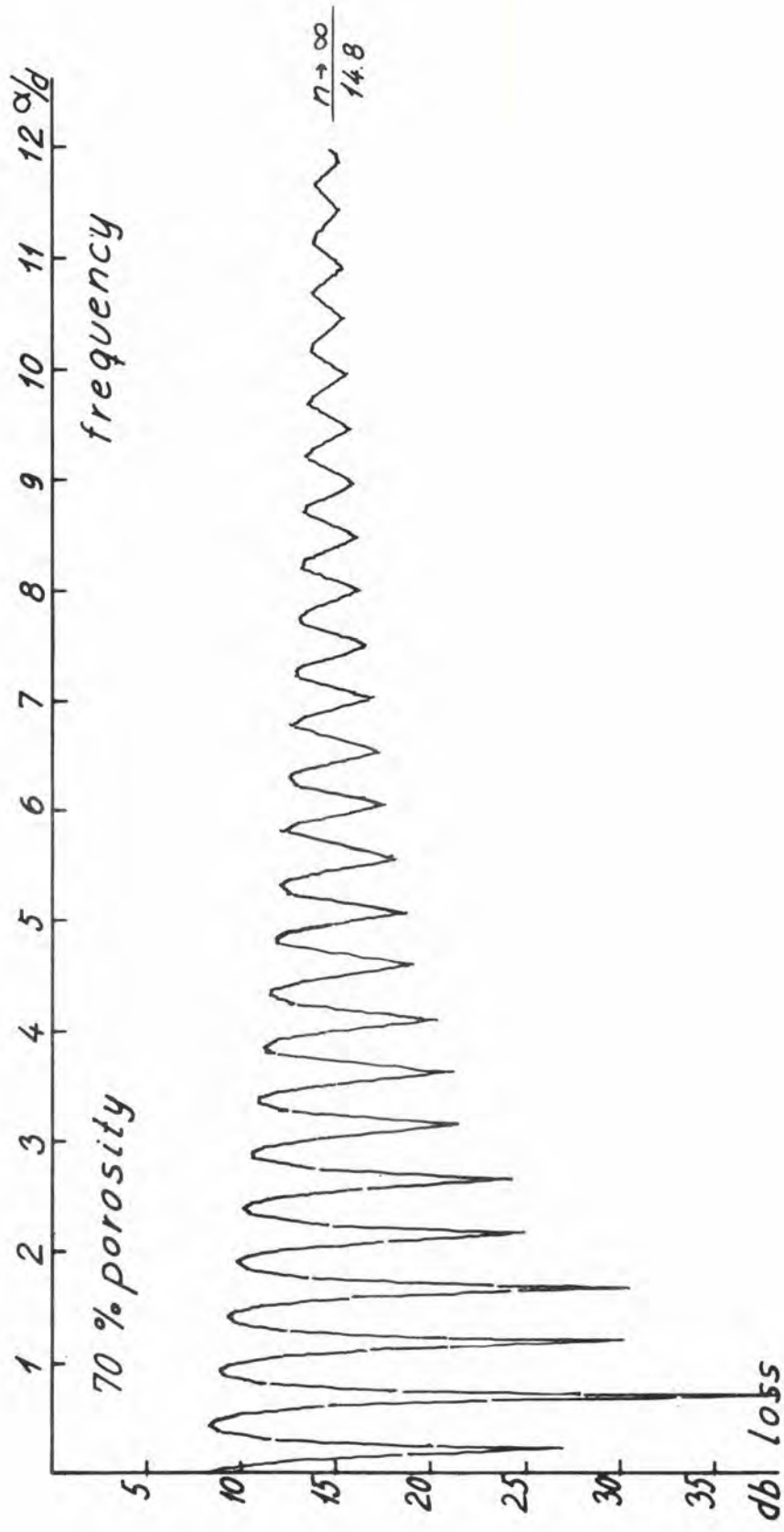FIG. 6 REFLECTION LOSS FOR VERTICAL INCIDENCE

FIG. 7 REFLECTION LOSS FOR VERTICAL INCIDENCE
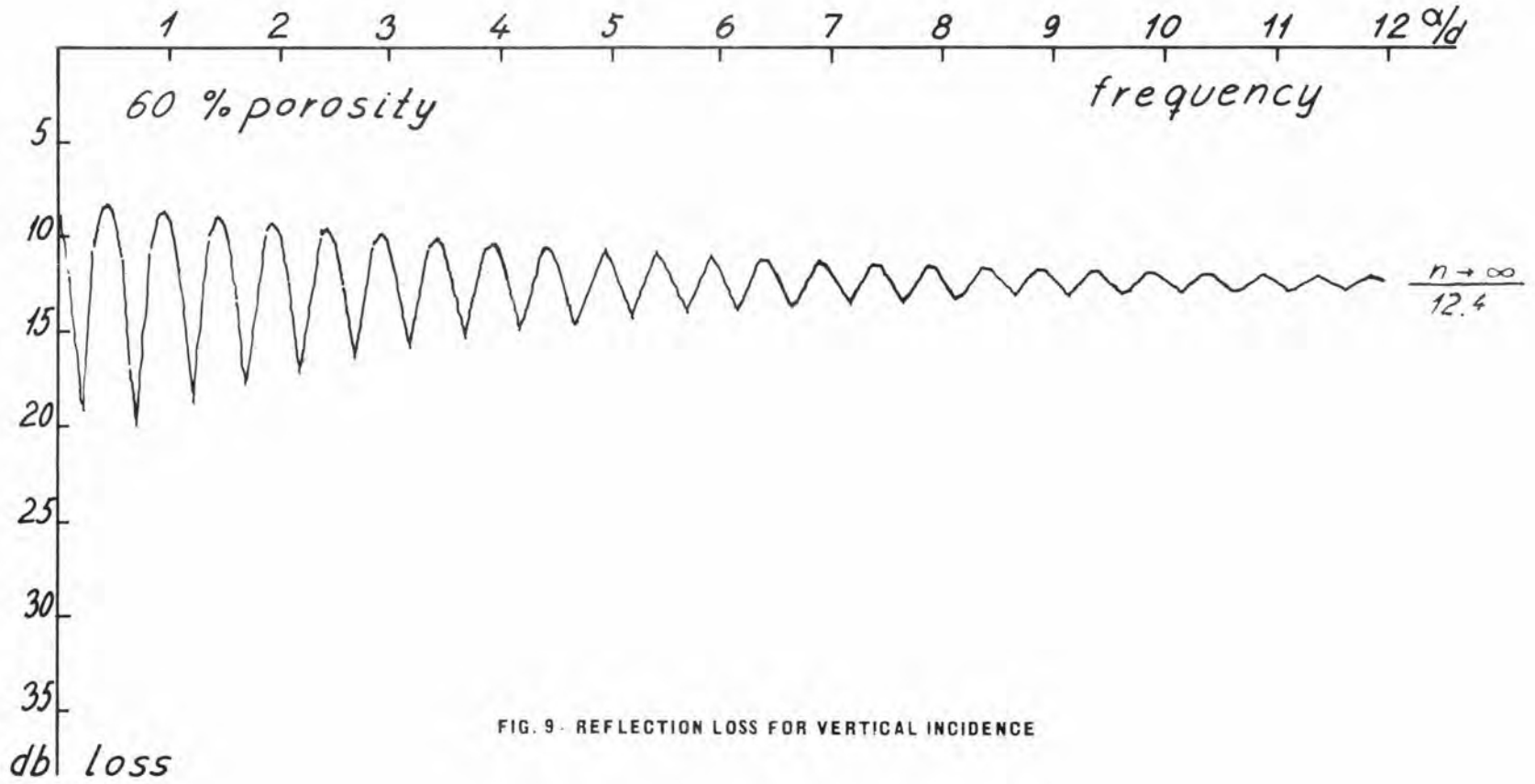
FIG. 8 REFLECTION LOSS FOR VERTICAL INCIDENCE

19

FIG. 9 - REFLECTION LOSS FOR VERTICAL INCIDENCE

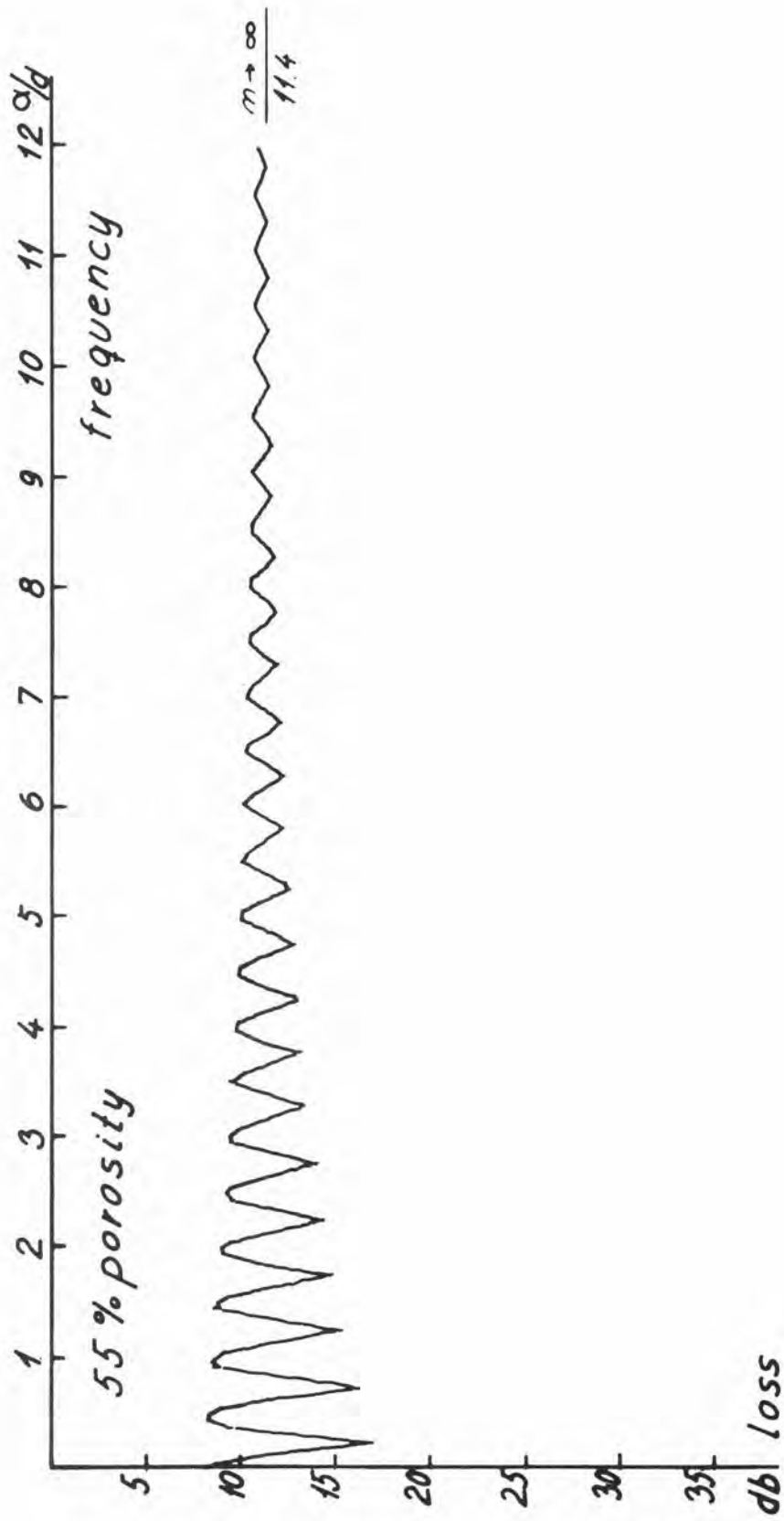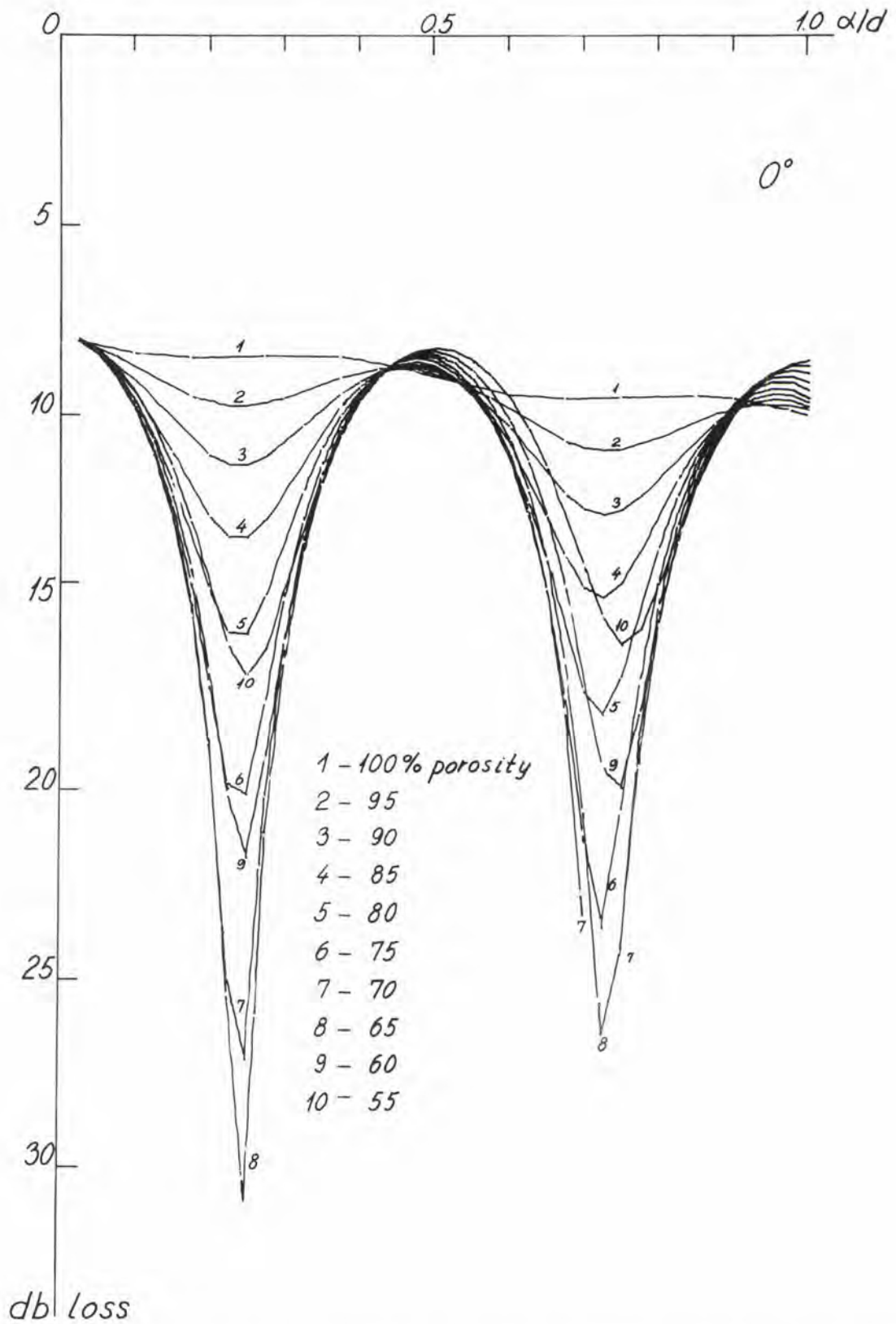**FIG. 9   REFLECTION LOSS FOR VERTICAL INCIDENCE**

20

FIG. 10 REFLECTION LOSS FOR VERTICAL INCIDENCE

FIG. II REFLECTION LOSS AS A FUNCTION OF LAYER THICKNESS FREQUENCY AND POROSITY

FIG. 12 REFLECTION LOSS AS A FUNCTION OF LAYER THICKNESS FREQUENCY AND POROSITY

1 – 100 % porosity
2 – 95
3 – 90
4 – 85
5 – 80
6 – 75
7 – 70
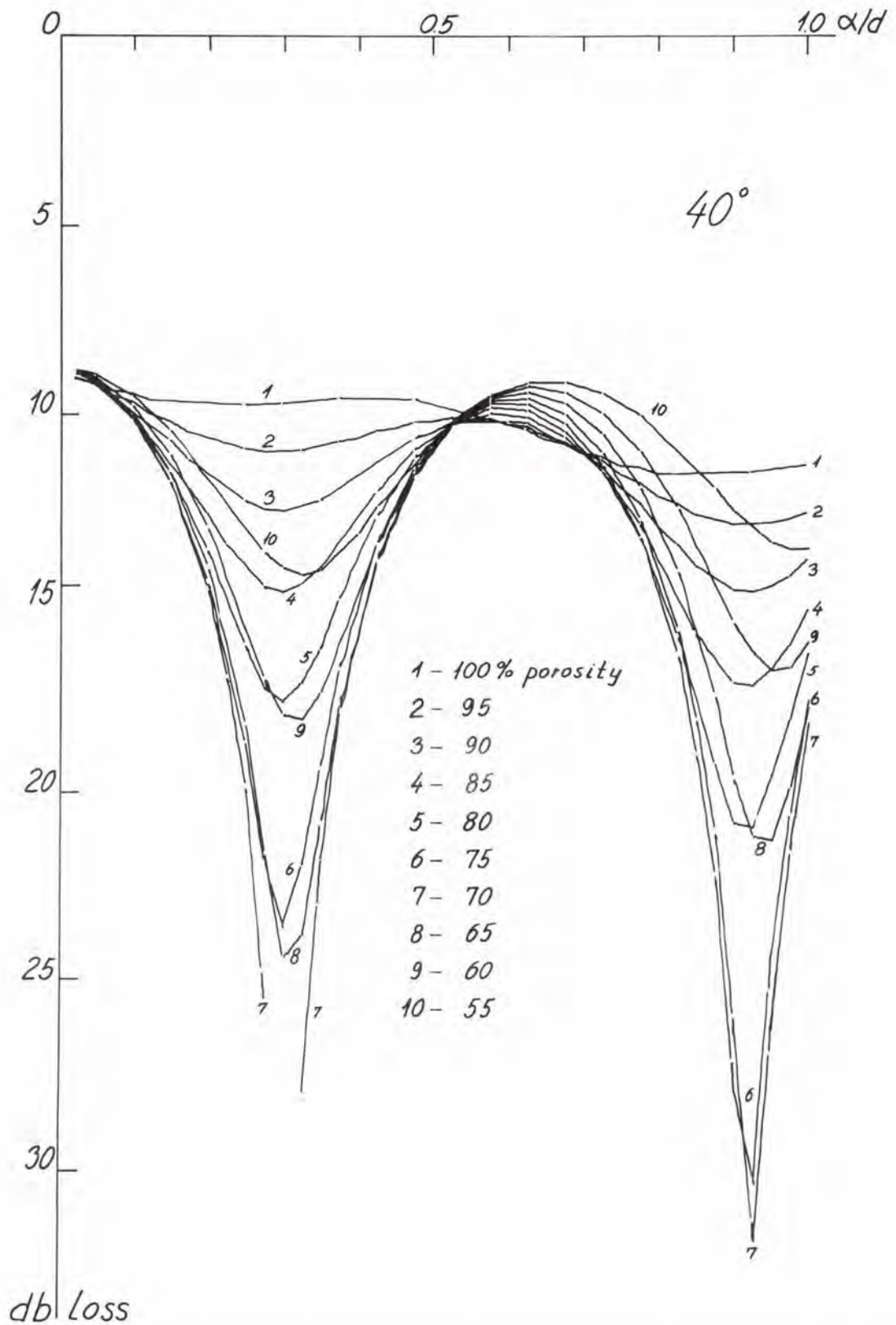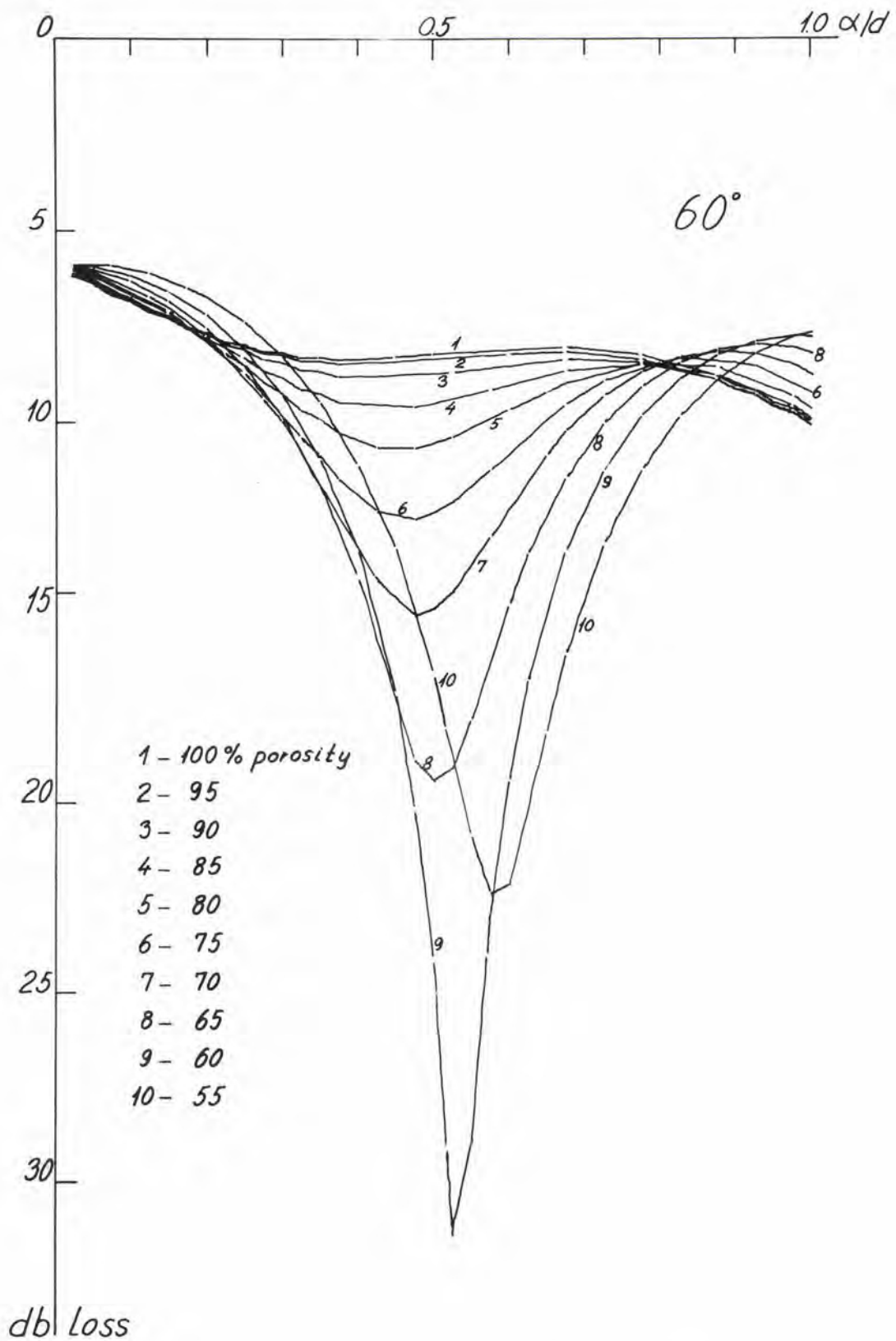8 – 65
9 – 60
10 – 55

40°

db loss

23

FIG. 13 REFLECTION LOSS AS A FUNCTION OF LAYER THICKNESS FREQUENCY AND POROSITY
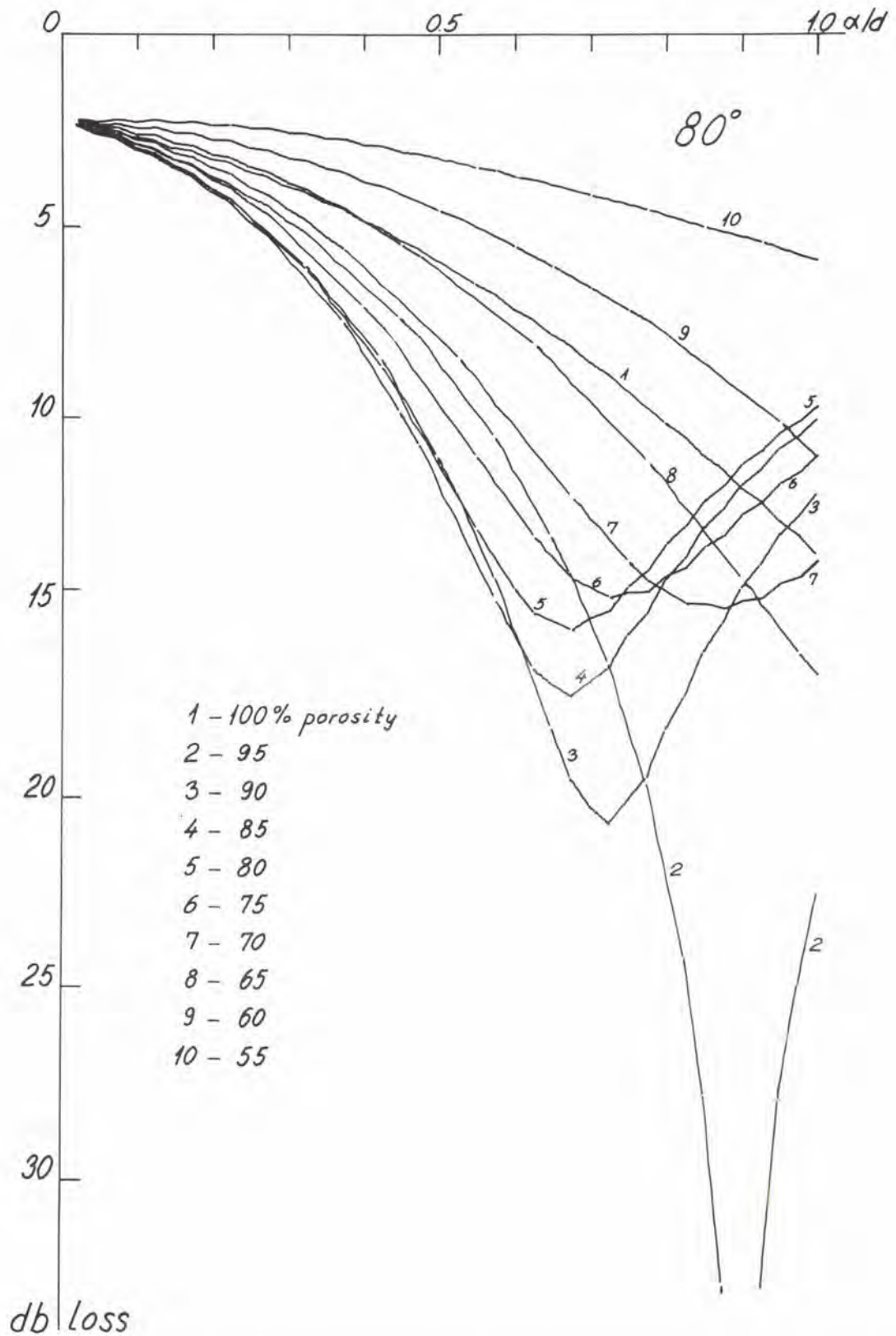
24

FIG. 14   REFLECTION LOSS AS A FUNCTION OF LAYER THICKNESS FREQUENCY AND POROSITY

The figure contains the following legend:

1 – 100 % porosity
2 – 95
3 – 90
4 – 85
5 – 80
6 – 75
7 – 70
8 – 65
9 – 60
10 – 55

Axis labels: horizontal axis marked 0, 0.5, 1.0 α/d; vertical axis marked 5, 10, 15, 20, 25, 30 db loss; annotation 80°.
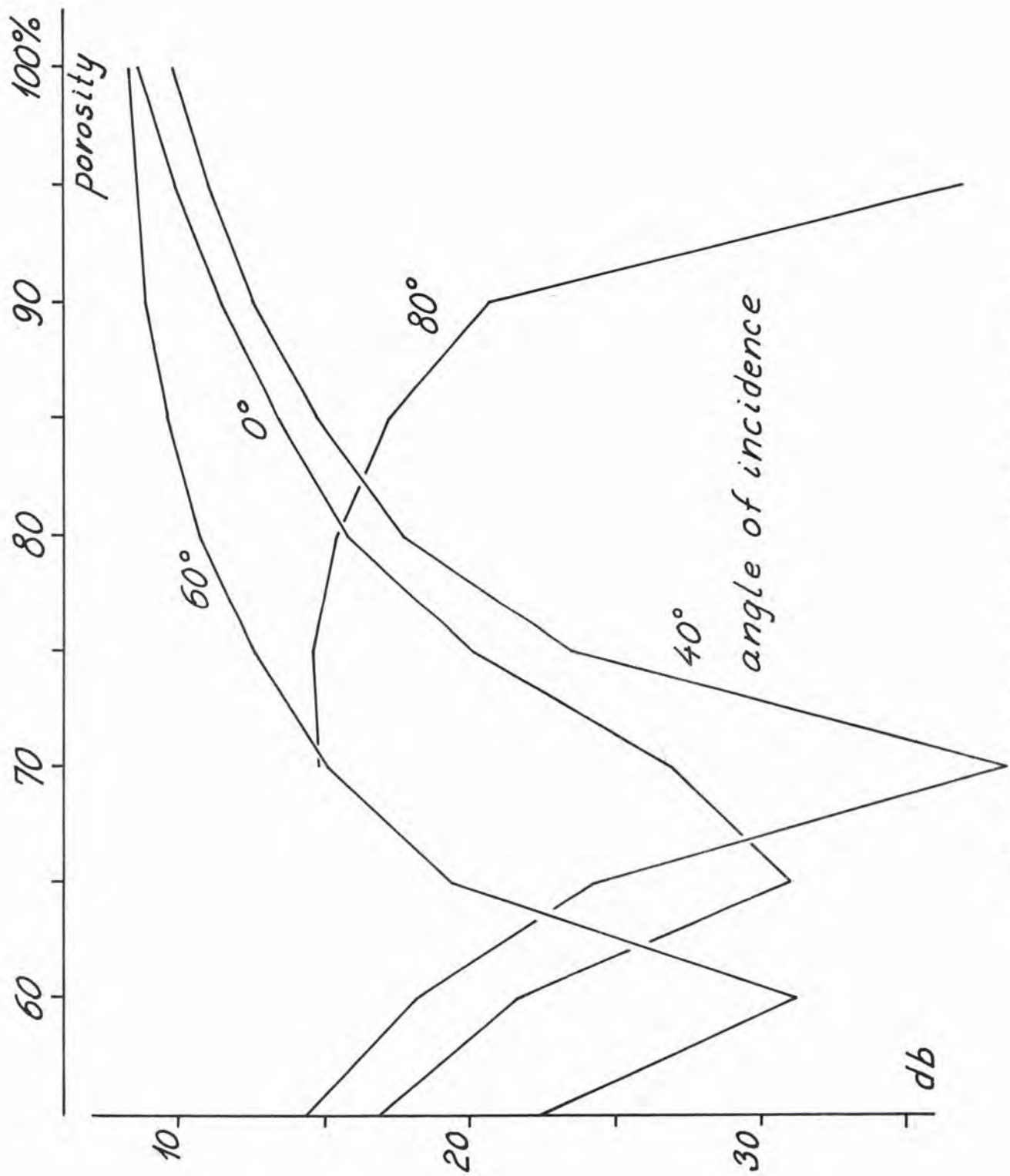
FIG. 15 MAXIMUM REFLECTION LOSS FOR $0 < \alpha/\lambda < 0.5$

26

FIG. 16 SHAPES OF THE REFLECTED SHOCK PULSE AT VELOCITY MINIMUM FOR DIFFERENT ANGLES OF INCIDENCE

27

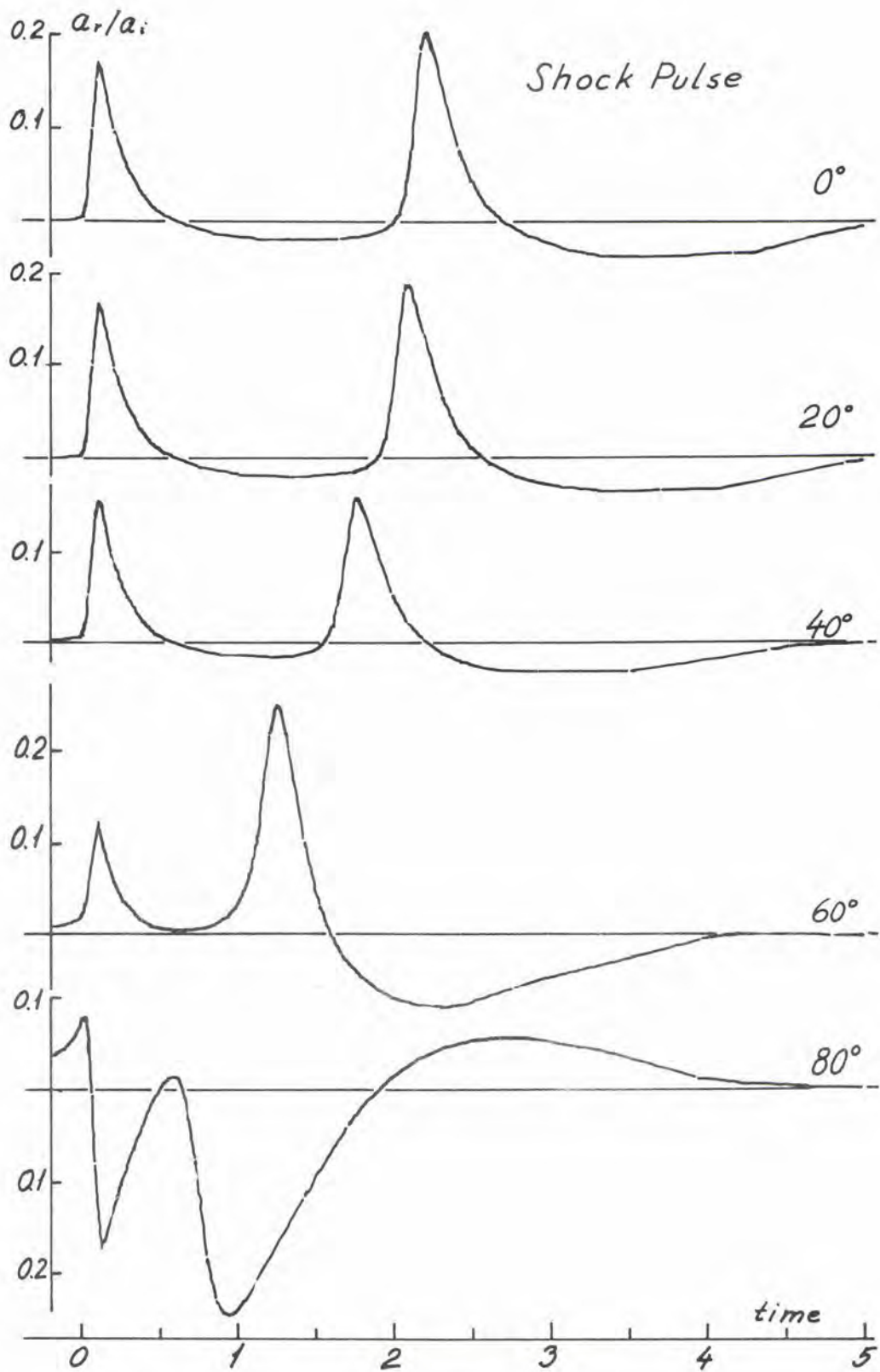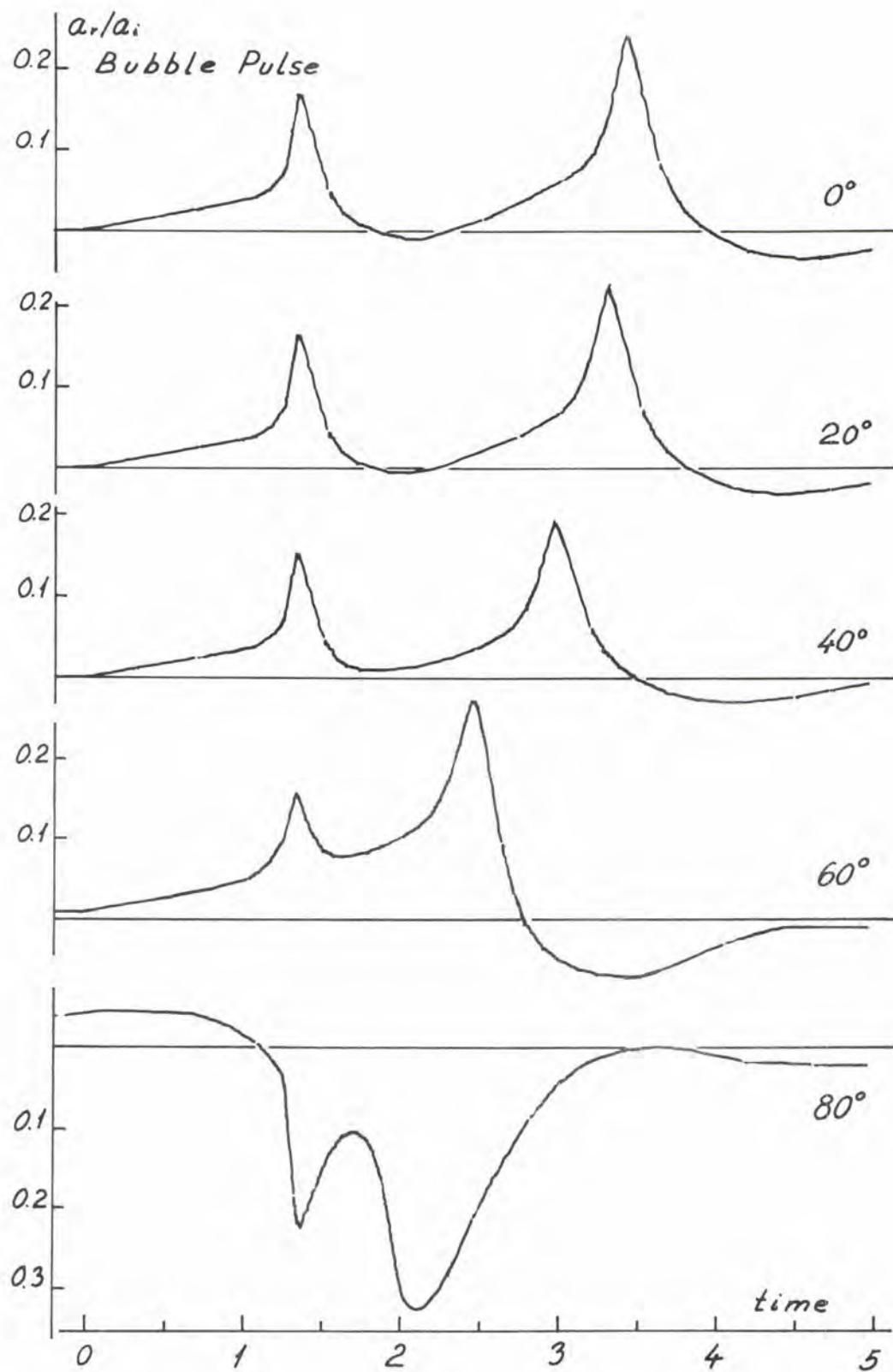**FIG. 17 SHAPES OF THE REFLECTED BUBBLE PULSE AT VELOCITY MINIMUM FOR DIFFERENT ANGLES OF INCIDENCE**

28
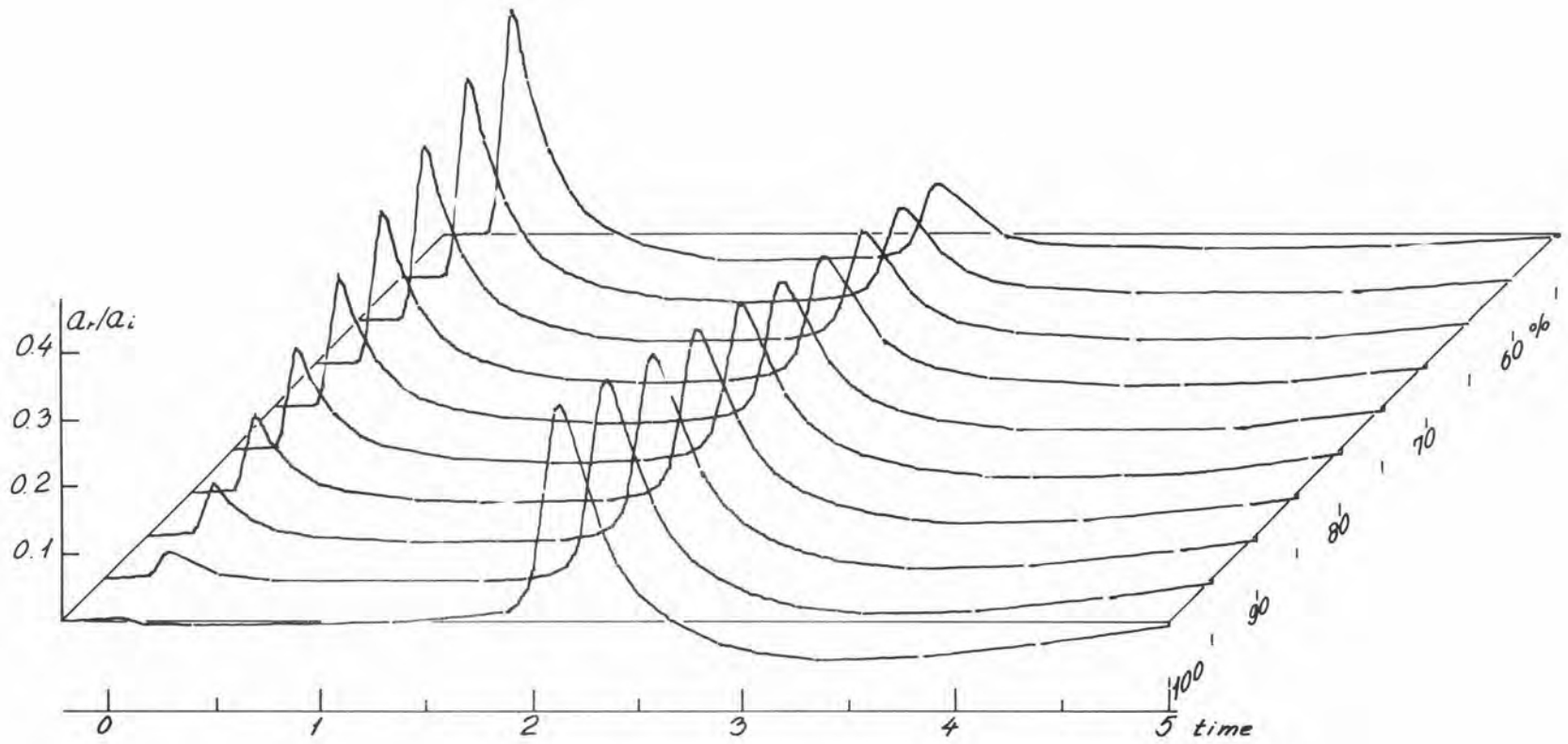
FIG. 18   SHAPES OF THE REFLECTED SHOCK PULSE FOR VERTICAL INCIDENCE AND DIFFERENT POROSITIES

29
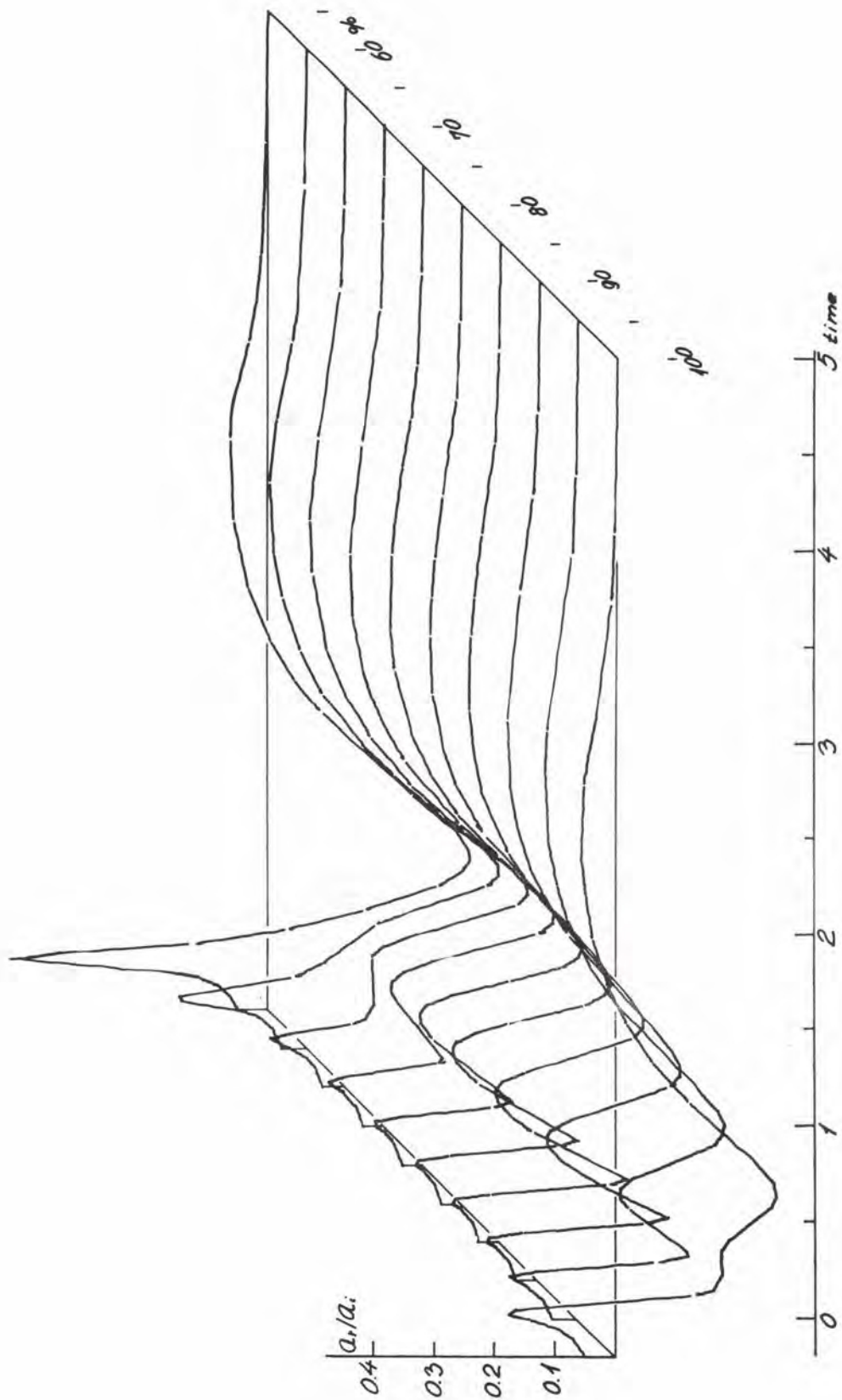
FIG. 19   SHAPES OF THE REFLECTED SHOCK PULSES FOR 80° INCIDENCE AND DIFFERENT POROSIES

30
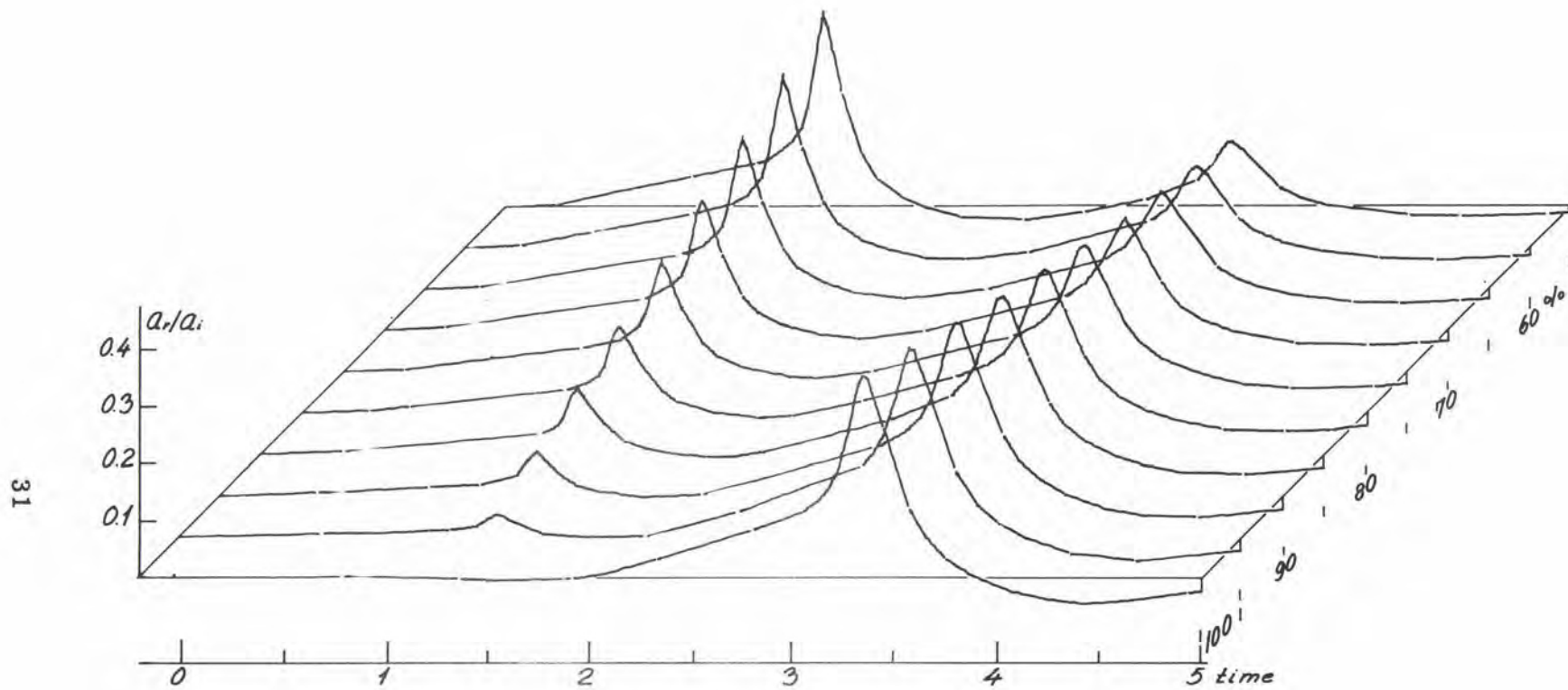
FIG. 20 SHAPES OF THE REFLECTED BUBBLE PULSES FOR VERTICAL INCIDENCE AND DIFFERENT POROSITIES
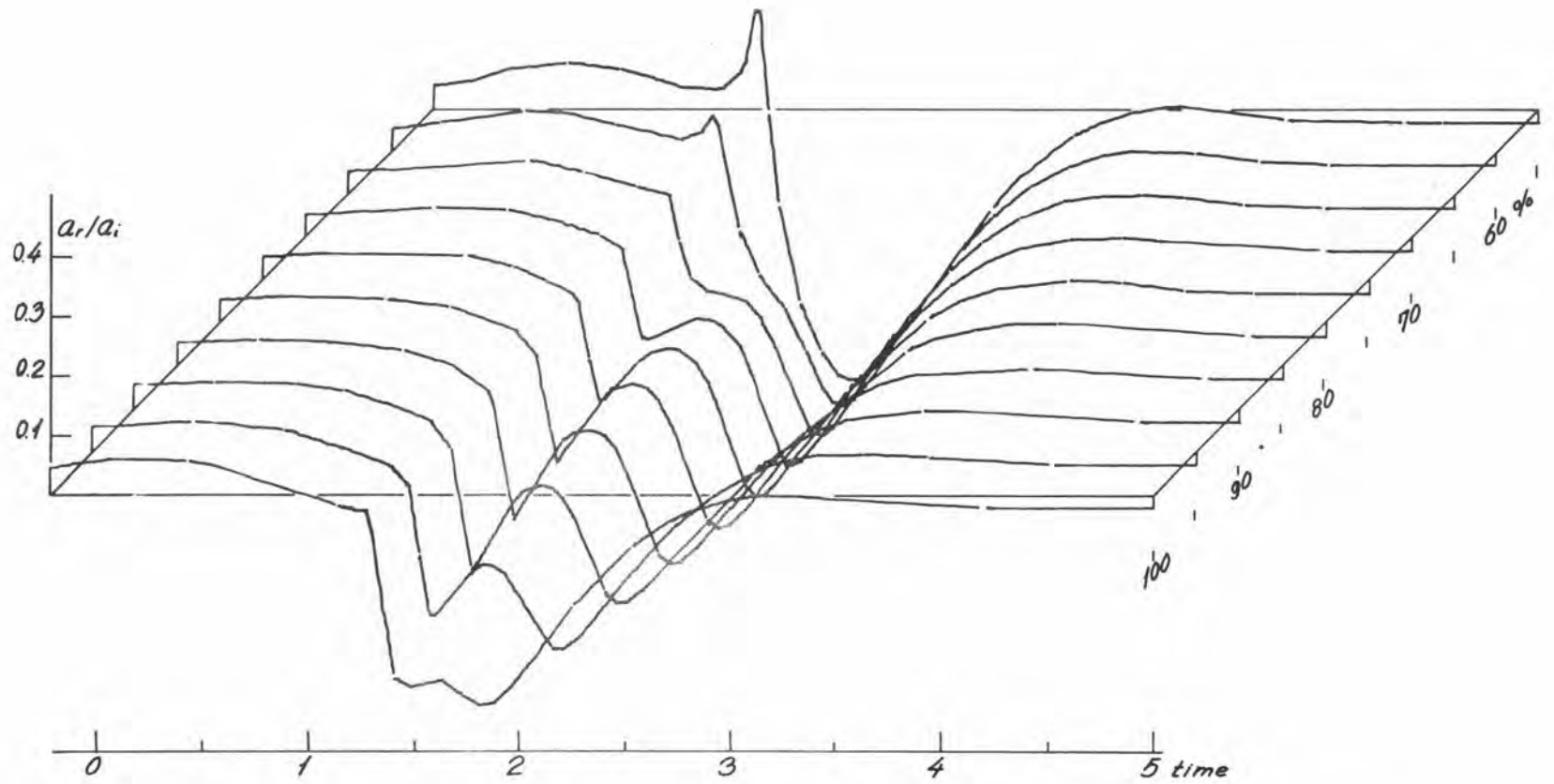
FIG. 21 SHAPES OF THE REFLECTED BUBBLE PULSES FOR 80° INCIDENCE AND DIFFERENT POROSITIES

Shock Pulse 0°

a_r/a_i
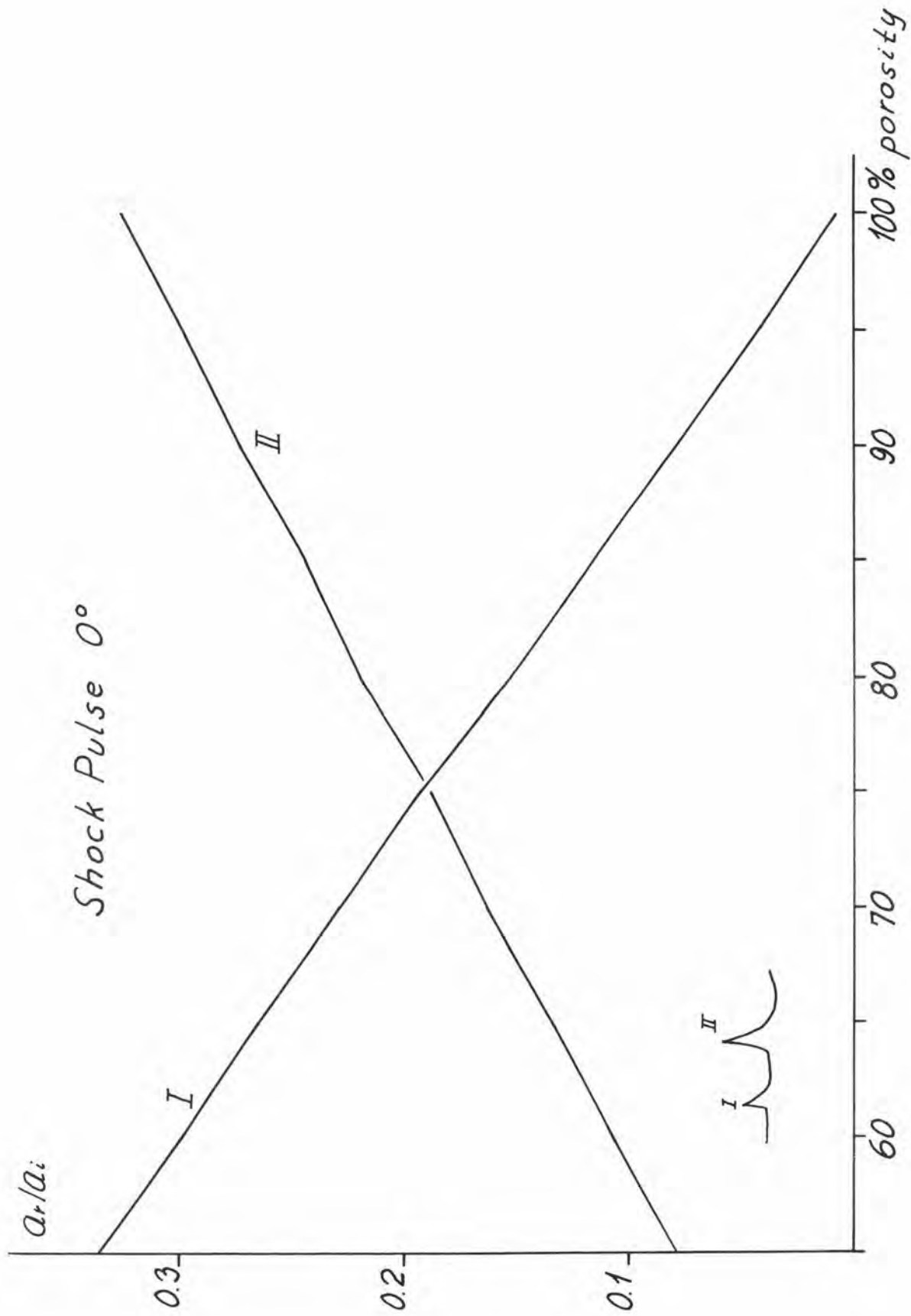
FIG. 22 PEAK AMPLITUDES FOR SHOCK PULSES AT 0° INCIDENCE

Shock pulse 80°

a_r/a_i
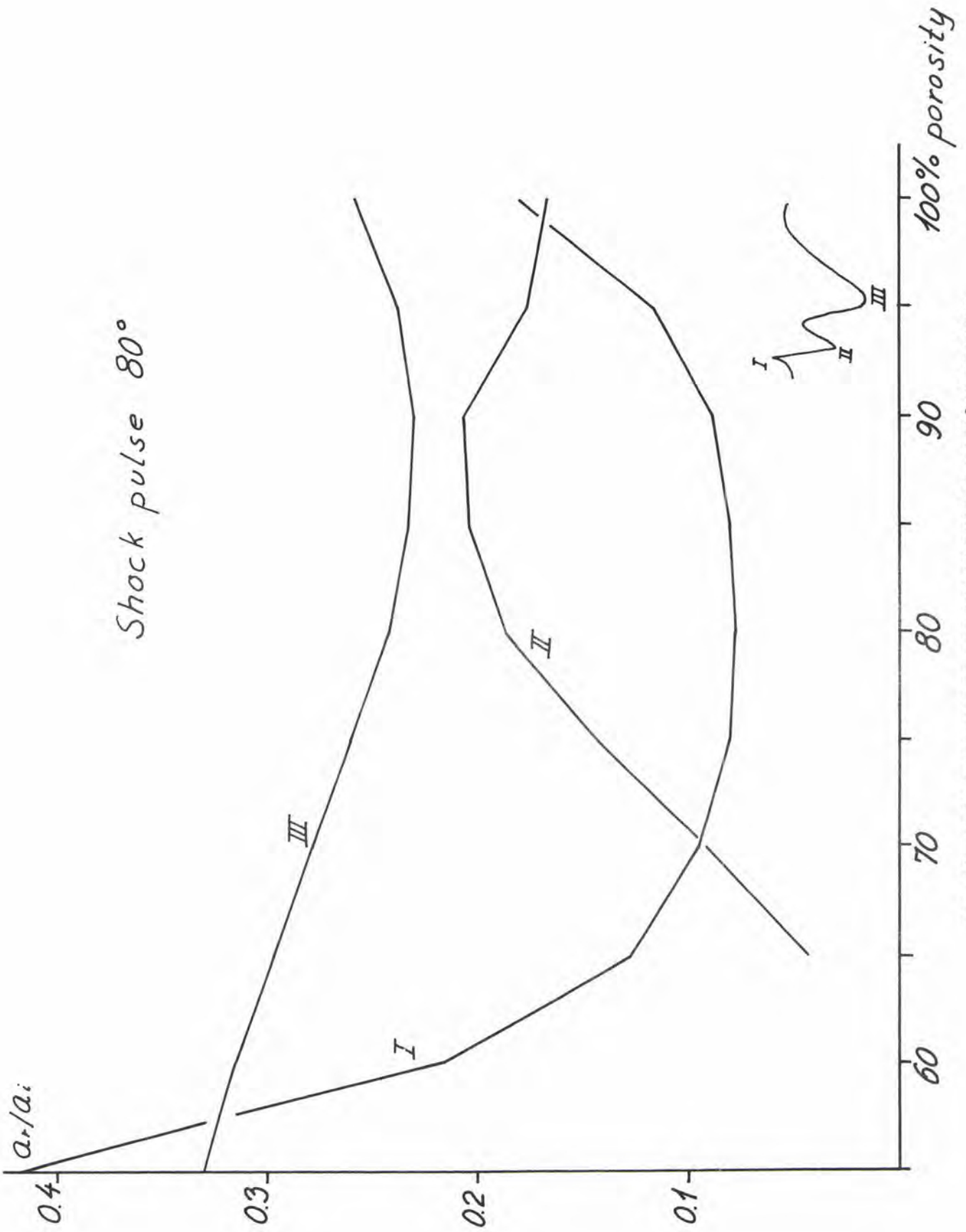
FIG. 23 PEAK AMPLITUDES FOR SHOCK PULSES AT 80° INCIDENCE

34

Bubble Pulse 0°

a_r/a_i
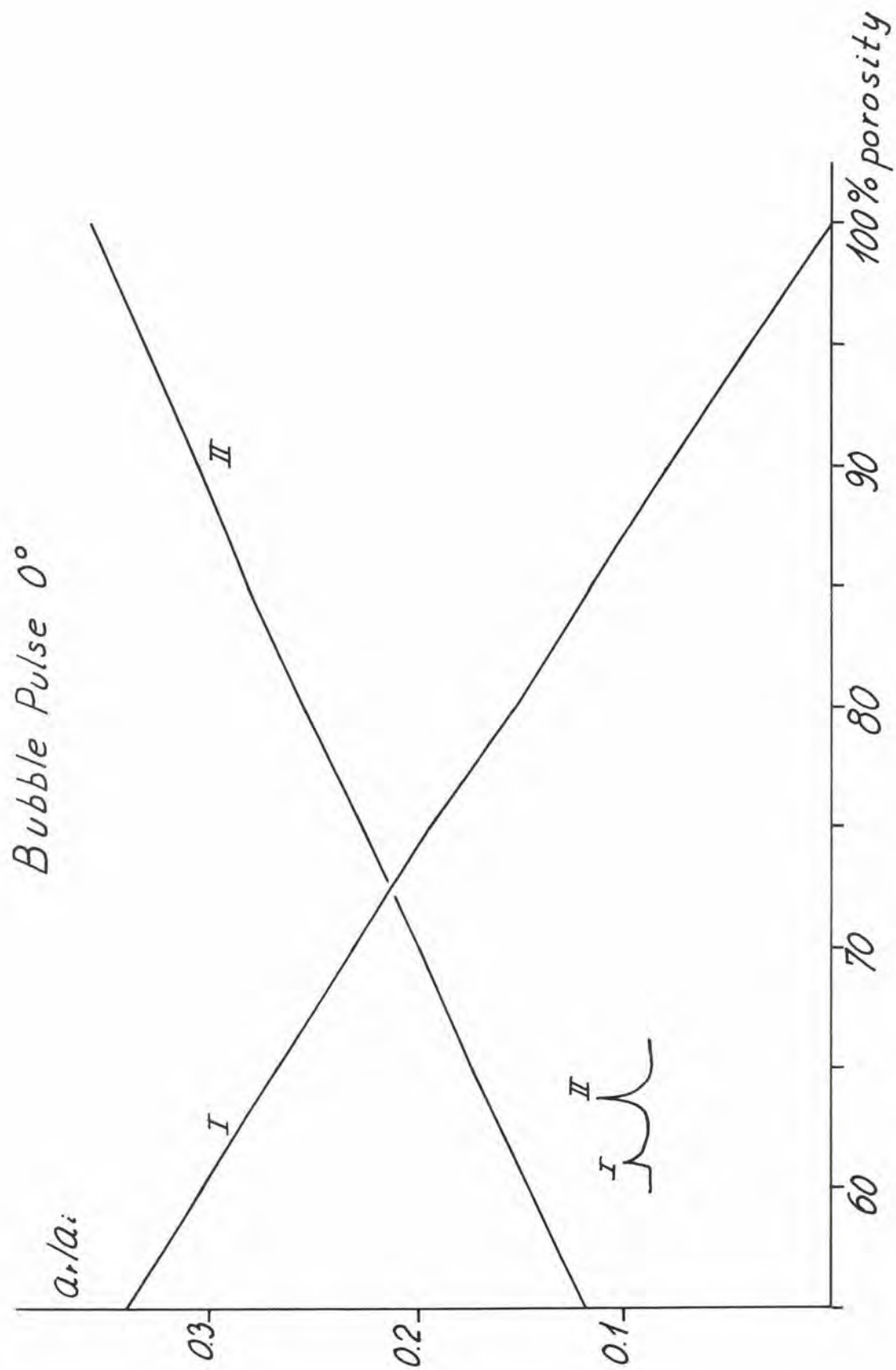
FIG. 24   PEAK AMPLITUDES FOR BUBBLE PULSES AT 0° INCIDENCE

35
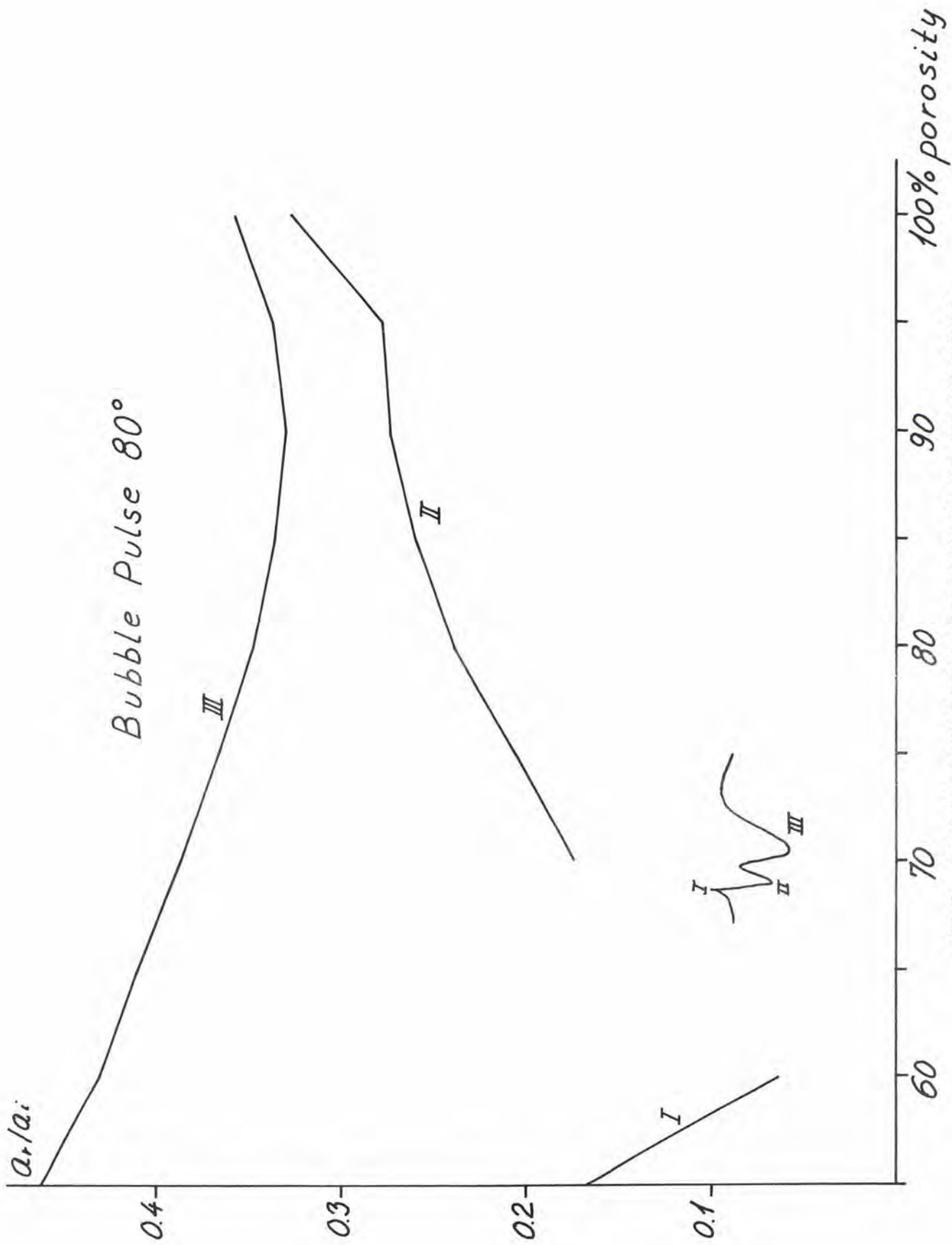
FIG. 25 PEAK AMPLITUDES FOR BUBBLE PULSES AT 80° INCIDENCE

APPENDIX

THEORY AND COMPUTATIONAL METHODS

The calculation of the reflection coefficient and the shape of a reflected pulse is, in the case of a general multi-layered bottom and an arbitrary incident pulse, only possible by the use of numerical methods in connection with a digital computer. Only a rather brief description will be given here and readers are referred to two previous reports (Refs. 5 & 6), where the methods are shown in greater detail.

In the case of reflection of plane waves from a layered sea floor it is possible to express all deformations and stresses by two sets of potentials satisfying the wave equation. The geometry of the layers is shown on Fig. 1.1.
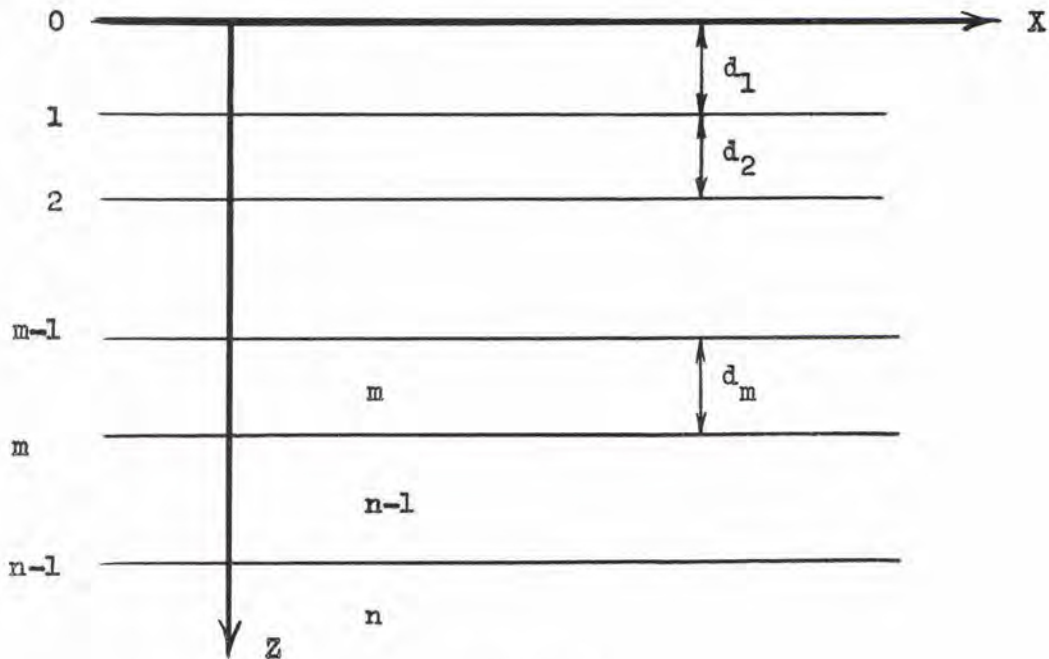
Fig. 1.1

For the mth layer the potentials will be

$$\phi_m = \left[A_m \, e^{-ik_n \cos\theta_m z} + B_m \, e^{ik_m \cos\theta_m z} \right] e^{i(\omega t - h x)}$$

$$\psi_m = \left[C_m \, e^{-i\kappa_m \cos\eta_m z} + D_m \, e^{i\kappa_m \cos\eta_m z} \right] e^{i(\omega t - h x)}$$

where A_m, B_m, C_m, D_m are constants.

k and κ are wave numbers for compressional and shear waves

θ and η are angles of incidence for compressional and shear waves

h is the common horizontal wave number

ω is the angular frequency.

By the use of the equations from the theory of elasticity, particle velocities and stresses can be calculated

$$\begin{bmatrix} \dot{u}/c \\ \dot{w}/c \\ \sigma \\ \tau \end{bmatrix} = \begin{bmatrix} t_{11} & t_{12} & t_{13} & t_{14} \\ t_{21} & t_{22} & t_{23} & t_{24} \\ t_{31} & t_{32} & t_{33} & t_{34} \\ t_{41} & t_{42} & t_{43} & t_{44} \end{bmatrix} \begin{bmatrix} A_m + B_m \\ A_m - B_m \\ C_m - D_m \\ C_m + D_m \end{bmatrix}$$

or, using a more convenient matrix notation,

$$\bar{S} = \bar{\bar{T}}(z) \cdot \bar{P},$$

$\dot{u}$ and $\dot{w}$ are the horizontal and vertical particle velocity,

σ and τ are the normal and shear stress,

t_{ij} are the 16 matrix elements depending on z, the elastic constants, damping and wave number, and

c is the horizontal phase velocity.

Placing the origin of the z axis at the $(m-1)^{th}$ interface we get, for z = 0 and z = d_m,

$$\bar{S}_{m-1} = \bar{\bar{T}}_m(0) \cdot \bar{P}_m$$

and

$$\bar{S}_m = \bar{\bar{T}}_m(dm) \cdot \bar{P}_m$$

where the indices for $\bar{S}$ refer to the interface, and the indices for $\bar{\bar{T}}$ and $\bar{P}$ refer to the layer. By elimination of $\bar{P}_m$ we get a relation between the condition on the top and the bottom of the layer.

$$\bar{S}_m = \bar{\bar{T}}_m(dm) \cdot \bar{\bar{T}}(0)^{-1} \cdot \bar{S}_{m-1}$$

or

$$\bar{S}_m = \bar{\bar{A}}_m \cdot \bar{S}_{m-1}$$

From the conditions of continuity, and successive use of the above equation,

$$\bar{S}_{n-1} = \bar{\bar{A}}_{n-1} \cdot \bar{\bar{A}}_{n-2} \cdots \cdot \bar{\bar{A}}_0 \cdot \bar{S}_0$$

or

$$\bar{P}_n = \bar{\bar{T}}_n^{-1}(0) \cdot \bar{\bar{A}}_{n-1} \cdot \bar{\bar{A}}_{n-2} \cdots \cdot \bar{\bar{A}}_0 \cdot \bar{S}_0$$

The damping is taken into account by the use of complex wave numbers.

In the two half spaces 0 and n, certain conditions have to be met. In the fluid , no shear stresses or shear waves can exist, which means that $\tau = C_o = D_o = 0$ and that, for the solid half space to ensure a limited potential for $z \to \infty$,

$$B_n = D_n = 0$$

We therefore get

$$\begin{bmatrix} A_n \\ A_n \\ C_n \\ C_n \end{bmatrix} = \begin{bmatrix} h_{11} & h_{12} & h_{13} & h_{14} \\ h_{21} & h_{22} & h_{23} & h_{24} \\ h_{31} & h_{32} & h_{33} & h_{34} \\ h_{41} & h_{42} & h_{43} & h_{44} \end{bmatrix} \times \begin{bmatrix} \dot{u}/c \\ \dot{w}/c \\ \sigma \\ 0 \end{bmatrix}$$

where the matrix $\overline{\overline{H}} = \overline{\overline{T}}_n(0)^{-1} \cdot \overline{\overline{A}}_{n-1} \ldots \ldots \overline{\overline{A}}_o$

Elimination of A_n, C_n and $\dot{u}/c$ yields

$$\dot{w}/c = - \frac{(h_{13} - h_{23})(h_{32} - h_{42}) - (h_{33} - h_{43})(h_{11} - h_{21})}{(h_{12} - h_{22})(h_{31} - h_{41}) - (h_{11} - h_{21})(h_{32} - h_{42})} \sigma$$

or

$$\sigma/\dot{w} = - Z_\ell$$

The impedance is defined as the ratio of the acoustic pressure to the normal component of particle velocity in a plane wave propagating in the direction of the positive axis. Therefore, $- \sigma/\dot{u}$ is the total layer impedance, the change in

40

sign being caused by the difference in defining the sign of stress and pressure.

So by the use of the well-known formula for the reflection coefficient we have

$$V = \frac{Z_i - Z_w}{Z_i + Z_w}$$

where $Z_w = \rho_0 \alpha_0 / \cos \theta_0$ is the impedance of the water.

V is generally complex and, amongst other things, is a function of frequency and represents the transfer function for the layered bottom.

The use of the theory for linear systems gives the reflected pulse

$$g(t) = \frac{1}{2\pi} \int_{-\infty}^{\infty} V(\omega) \cdot F(\omega) \, e^{i\omega t} \, d\omega \quad,$$

where $F(\omega) = \int_{-\infty}^{\infty} f(t) \, e^{-i\omega t} \, dt$ and $f(t)$ is the incident pulse.

To be able to handle both numerical and analytical reflection coefficients and pulse shapes, the two integrals have to be evaluated by numerical methods. Usual quadrature is not possible because of the factor $e^{\pm i\omega t}$, but approximating the other factor of the integrand by a system of trapezoids and using double differentiation, the integrand will be a sequence of Dirac pulses, which can be summed. For example, for the second integral

$$-\omega^2 \, F(\omega) = \int f''(t) \, e^{-i\omega t} \, dt = \int \sum_j k_j \, \delta(t-t_j) \, e^{-i\omega t} \, dt$$

$$F(\omega) = -\frac{1}{\omega^2} \sum_j k_j \, e^{-i\omega t_j}$$

41

The programmes to calculate $V(\omega, \theta_o)$ and $g(t)$ are written in ALGOL for the Centre's ELLIOTT 503 digital computer. To speed up publication of the reports as much as possible, the curve drawing and plotting has been done on the Centre's "BENSON-FRANCE ELECTROPLOTTER".

DISTRIBUTION LIST

MINISTRIES OF DEFENCE

Minister of Defence Brussels, Belgium	10 copies
Department of National Defence Ottawa, Canada	10 copies
Chief of Defence Copenhagen, Denmark	10 copies
Minister of National Defence Paris, France	10 copies
Minister of Defence Federal Republic of Germany Bonn, Germany	12 copies
Minister of Defence Athens, Greece	10 copies
Minister of National Defence Rome, Italy	10 copies
Minister of National Defence The Hague, Netherlands	10 copies
Minister of National Defence Oslo, Norway	10 copies
Minister of National Defence Lisbon, Portugal	10 copies
Minister of National Defence Ankara, Turkey	10 copies
Minister of Defence London, England, U.K.	20 copies
SECDEF United States (through USNLO to SACLANTCEN, ONR, London)	70 copies

NATO AUTHORITIES

Standing Group NATO Washington D.C. 20301	3 copies
SECGEN NATO (through SGREP) Paris, France	5 copies
ASG for Scientific Affairs NATO Paris, France	1 copy
SACLANT Norfolk, Virginia 23511	3 copies
SACEUR Paris, France	7 copies
CINCHAN Ft. Southwick, Fareham England	1 copy
SACLANTREPEUR Paris, France	1 copy
COMAIRCHAN Northwood, England	1 copy
CINCAFMED Malta G.C.	1 copy
CINCEASTLANT Eastbury Park Northwood, England	1 copy
CINCWESTLANT Norfolk, Virginia 23511	1 copy
COMMAIREASTLANT Northwood, England	1 copy
COMSUBEASTLANT Ft. Blockhouse Gosport, England	1 copy

COMCANLANT H.M.C. Dockyard Halifax, Canada	1 copy
COMOCEANLANT Norfolk, Virginia 23511	1 copy
COMEDCENT Naples, Italy	1 copy
COMEDSOUEAST Malta G.C.	1 copy
COMSUBACLANT Norfolk, Virginia 23511	1 copy
COMSUBMED Malta G.C.	1 copy
Commander TASK FORCE 442 FPO, N.Y. 09521	1 copy
SHAPE T.C. The Hague, Netherlands	1 copy

SCIENTIFIC COMMITTEE OF NATIONAL REPRESENTATIVES FOR SACLANTCEN

SCNR Belgium	1 copy
SCNR Canada	1 copy
SCNR Denmark	1 copy
SCNR France	1 copy
SCNR Germany	1 copy
SCNR Greece	1 copy
SCNR Italy	1 copy
SCNR Netherlands	1 copy
SCNR Norway	1 copy
SCNR Turkey	1 copy
SCNR United Kingdom	1 copy
SCNR United States	1 copy

NATIONAL LIAISON OFFICERS FOR SACLANTCEN

NLO France	1 copy
NLO Italy	1 copy
NLO Portugal	1 copy
NLO United States	1 copy

NATIONAL LIAISON REPRESENTATIVES TO SACLANT

NLR Belgium	1 copy
NLR Canada	1 copy
NLR Denmark	1 copy
NLR France	1 copy
NLR Germany	1 copy
NLR Greece	1 copy
NLR Italy	1 copy
NLR Netherlands	1 copy
NLR Norway	1 copy
NLR Portugal	1 copy
NLR Turkey	1 copy
NLR United Kingdom	1 copy